

Tools Made of Light-The
Physics Nobel Prize 2018 1

Polyphenolic Malabaricones
for Anti-Cancer 13

Biodosimetry Techniques and
Biological Indicators 22



Bi-monthly • September - October • 2018

ISSN: 0976-2108

BARC

NEWSLETTER

Surface morphology of electro-deposited Boron

SEI 20.00 kV Mag: 1500

10 μ m

CONTENTS

Editorial Committee

Chairman

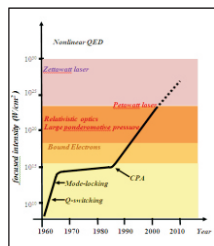
Dr. G.K. Dey
Materials Group

Editor

Dr. G. Ravi Kumar
SIRD

Members

Dr. G. Rami Reddy, RSD
Dr. A.K. Tyagi, Chemistry Divn.
Dr. S. Kannan, FCD
Dr. C.P. Kaushik, WMD
Dr. S. Mukhopadhyay,
Seismology Divn.
Dr. S.M. Yusuf, SSPD
Dr. B.K. Sapra, RP&AD
Dr. J.B. Singh, MMD
Dr. S.K. Sandur, RB&HSD
Dr. R. Mittal, SSPD
Dr. Smt. S. Mukhopadhyay, ChED

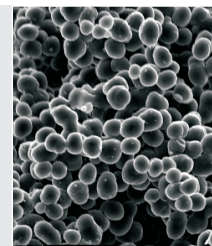


Tools Made of Light-The Physics Nobel Prize 2018
Paramita Deb

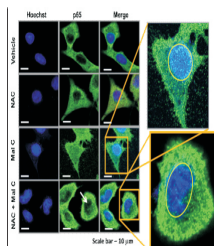
1

Preparation of High Purity Boron by Molten Salt Electroextraction

Sanjib Majumdar, S.S. Molke, A.D. Sonawane, S.K. Gavai,
R. Vanneldas, P.S. Yadav, P.B. Shelke, Vivekanand Kain and
Madangopal Krishnan



8



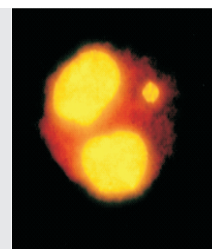
Synthesis and Evaluation of Polyphenolic Malabaricones for their Anti-Cancer Potential

Mrityunjay Tyagi, Kshma Kundu, Ajay Kumar Bauri,
Birija Sankar Patro and Sandip Kumar Nayak

13

Biodosimetry techniques and the Biological Indicators of Radiation Exposure in Humans

Nagesh N. Bhat, Rajesh Chaurasia, Usha Yadav, B. K. Sapra



22

Tools Made of Light-The Physics Nobel Prize 2018

Paramita Deb

High Pressure & Synchrotron Radiation Physics Division, Physics Group
Bhabha Atomic Research Centre, Trombay, Mumbai – 400085

Abstract

The Nobel Prize winners have successfully used those properties of lasers that have seldom been used previously. *Arthur Ashkin* used the property that light can exert pressure. The pressure exerted is proportional to the intensity of light. Therefore lasers with its high intensity could exert the pressure on tiny objects. *Gérard Mourou* and *Donna Strickland* used the property, that lasers are not strictly monochromatic. The spectral profile of the laser does have a fairly large bandwidth that can be manipulated. *Arthur Ashkin* realized that a laser would be the perfect tool for getting beams of light to move small particles. *Gérard Mourou* and *Donna Strickland* paved the way towards the shortest and most intense laser pulses created till date. The Royal Swedish Academy has honored the three physicists for their “ground breaking inventions in the field of laser physics”. *Arthur Ashkin* [1] has been honored for his invention of optical tweezers, that trap and manipulate particles and living cells. *Gérard Mourou* and *Donna Strickland* together [2] have been honored for developing “chirped pulse amplification” (CPA) in which a laser pulse is stretched amplified and then compressed to increase its power.

Keywords: Lasers, Ultra short Pulse, Chirped pulse, Stretcher/Compressor, Peak power, Optical tweezers, Light pressure, Spectral bandwidth.

Introduction

The inventions being honored, is in the realm of laser physics. Since the invention of the laser in 1958, the Nobel Prizes that have been awarded, for the work on lasers or for the work with lasers, is quite extensive. However, the full potential of lasers has not yet been realized. The 2018 Physics Nobel Prize is shared by three physicists (*Arthur Ashkin*, *Gérard Mourou* and *Donna Strickland*), who have proved beyond doubt that the laser is a fantastic tool made of light.

Lasers are presently being used routinely in scientific, military, medical and commercial applications. Some of the applications are laser cutting, welding and drilling. Lasers are used for photo-lithography, range finders, barcode readers, pointers and holography. In the entertainment industry lasers are used for lighting displays and other visual effects. In the medical field lasers are used for removing scar, tattoos and hair. The laser is used as a scalpel for soft tissue surgery. It is used

for the correction of myopia, and the removal of tumors. It is used in cancer treatment and in dentistry too. In scientific research, lasers are used as a spectroscopic tool, which is a must in all laboratories. Lasers are routinely being used for Raman spectroscopy, atmospheric remote sensing, holography, LIDAR ('light' and 'radar') applications, photochemistry and biochemistry. The high brightness, high intensity, high mono-chromaticity, and very low beam divergence and coherence are all properties which allow for these specialized applications. Lasers have penetrated every aspect of our lives. In fact we have forgotten that “laser” is not a word but an acronym (Light Amplification by Stimulated Emission of Radiation – LASER).

In the following paragraphs a flavor of the CPA technology will be presented. This technique has been researched and developed at BARC.

Ultra short pulse and dispersion management

The idea of chirped pulse amplification (CPA) was proposed

many years earlier for a different problem altogether. It was used to solve the problem in radar systems. The main issue in designing a good radar system is the capability of the system to resolve, two tiny objects, at a long range with a very small separation between them. The technique of pulse compression is used for efficient radar transmission. By transmitting a wide pulse in which the carrier frequency is modulated and then by passing the received signal through a matched filter to accumulate the energy into a short pulse, a time compression is brought about. However transferring the idea from longer radio waves to shorter optical waves was not a trivial task. It was difficult in theory and in practice. The CPA technique enabled the emission of very intense ultra short pulses of light, using an elegant method, to avoid the risk of destroying the amplifying material. *Gérard Mourou* and *Donna Strickland* got the breakthrough, when a stretcher and a matched compressor were put together to obtain a very short and intense

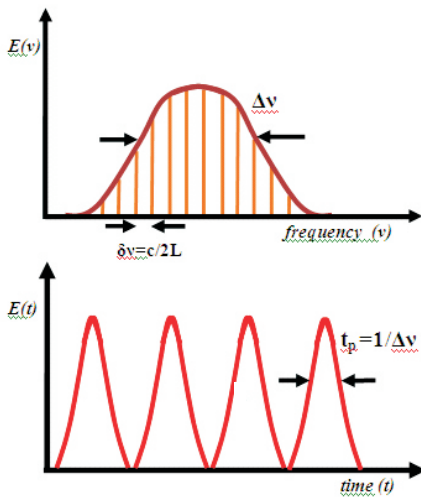


Fig.1. The output optical signal, schematic, from a mode-locked laser oscillator. Electric field amplitude $E(v)$ is a function of frequency v . $E(t)$ is its Fourier transform as a function of time t . δv is the mode spacing and Δv is the emission bandwidth, that is the full width at half maximum of the spectrum (top graph).

amplified pulse of light. Some of the issues that need to be understood are the phenomenon that govern the generation of an ultra-short optical pulse (of the order of pico-second and femto-second) and why these short pulses cannot be amplified directly and which processes prevent the direct optical amplification.

By the uncertainty principle, an ultra short pulse in the time domain must have a correspondingly broad spectrum in the spectral domain. It is therefore necessary to establish that the gain medium has a sufficiently broad bandwidth to amplify the short pulse, and other components (like mirrors, windows, lenses, modulators, etc) also are sufficiently broad band in their reflection or transmission responses, to transmit the pulses without filtering the pulse spectrum. Ultra short pulses are generated by the technique of mode-locking and in general the radiation in a laser oscillator cavity resonates in discrete longitudinal modes. More than one longitudinal mode can extract energy from the oscillator

active (gain) medium. The finite number of oscillating laser modes are separated in frequency by $\delta v=c/2L$, where L is the oscillator cavity length and ' c ' is the speed of light. The goal of mode locking is to ensure that the oscillating laser modes are locked in phase. Under these conditions the temporal output (Fig.1) will be a train of pulses separated by the cavity round trip time T . The duration of the pulse t_p , is related to the width (Δv) of the laser emission, expressed as $\Delta v t_p = k$. The factor k depends on the pulse shape. For Gaussian pulses $k=0.441$ and for hyperbolic secant pulses $k=0.315$. In order to generate ultra short pulses in the time domain, it is necessary to obtain mode-locked laser output with a broad spectral width in the frequency (or wavelength) domain. Therefore the shortest optical pulses are obtained from gain media with broad spectral ($v=c/\lambda$ and $\Delta v=(c/\lambda^2)\Delta\lambda$) gain profiles. Ti:Sapphire is a popular active media or gain media that is used in optical oscillators. The emission line width of such a medium is in the range of 170nm ($\Delta\lambda$). Even Nd:glass is a frequently used medium for the generation of femto-second range mode locked pulses, though the emission line width is much smaller ($\Delta\lambda=35$ nm).

With mode-locking one may generate pico-second range pulses, but to generate pulses shorter than a picoseconds (femto-second range), the spectral profile of the pulse circulating in the oscillator cavity has to be adjusted or managed properly. Progress in ultra fast optics has relied extensively on the development of ways to characterize and manipulate dispersion. Dispersion is a phenomenon where the phase velocity of a wave depends on its frequency (or wavelength). Phase velocity (' v ') in a uniform medium is written as $v=c/n$ where ' c ' is the speed

of light and ' n ' is the refractive index of the material. For visible light, the refractive index, ' n ', of most transparent materials decrease with increasing wavelength. That means $1 < n(\lambda_{red}) < n(\lambda_{yellow}) < n(\lambda_{blue})$ or alternatively it means that $dn/d\lambda < 0$. Here the medium is said to have normal dispersion. If the refractive index increases with increasing wavelength (for example in the ultraviolet wavelengths) the medium is said to have anomalous dispersion. Another quantity that is required in the subject of dispersion is the group velocity. Group velocity of the wave is the rate at which, changes in the amplitude (the envelope of the wave) will propagate. The group velocity v_g is expressed as $v_g=v/[1-(\lambda/n)(dn/d\lambda)]$. As can be seen, the group velocity is a function of the wave frequency or wavelength. This results in group velocity dispersion (GVD) which causes a short pulse of light to spread in time as a result of different frequency components of the pulse travelling at different velocities in a medium. Thus the consequence of dispersion manifests itself as a temporal effect. This phenomenon that causes different wavelengths in a wave packet to travel at different speeds/velocities, broadens the ultra short pulse temporally as it circulates in the cavity. The spectral width of the pulse is inversely proportional to the minimum temporal duration and so as pulses become shorter, they become more susceptible to GVD. Clearly excessive GVD will prevent the generation of short pulses and so it should be minimized.

Now in a laser oscillator cavity there is one more phenomenon taking place. Suppose that a laser is mode locked and each pulse in the train of pulses is about 1ps. The intra cavity pulse energy would be about 10nJ-1μJ, then the peak powers reach the range of

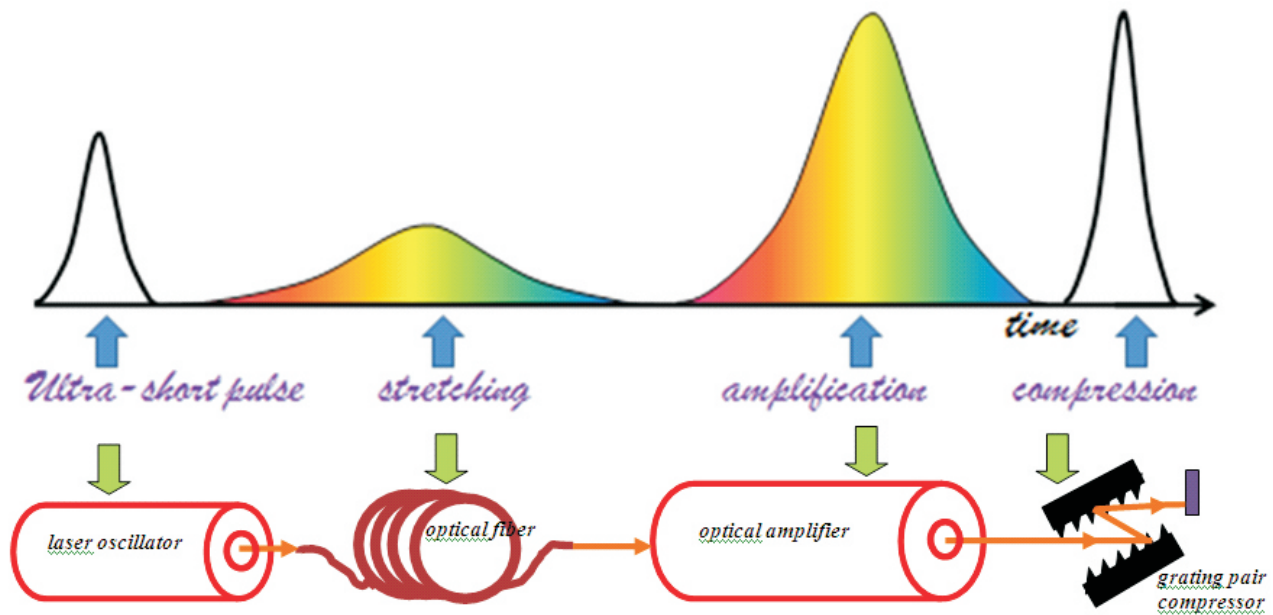


Fig.2. Schematic of the CPA concept. The oscillator produces a short pulse, which is then passed through an optical fiber where the pulse is stretched (1st communication by D. Strickland & G. Mourou) from femto-seconds to nearly a nano-second. The intensity is low enough to be amplified in an amplifier. Energy is extracted from the amplifier without pulse distortions or amplifier material damage. After energy extraction the pulse is compressed to nearly its original temporal width.

10KW to 1MW. Most cavity radiation is generally focused to about 100µm, making the intensity inside the cavity reach level of 10^8 - 10^{10} W/cm². At these intensities the refractive index of the intra-cavity medium can become non-linear due to optical Kerr effect, and this gives rise to self phase modulation (SPM). SPM causes the pulse spectrum to broaden, which can increase the loss at any spectral filter in the laser oscillator cavity if it is not broad band enough. The added spectrum or frequency chirp, should make the circulating pulse shorter, but a shorter pulse is more prone to GVD and therefore detrimental to the generation of a short temporal pulse. The interaction of SPM and GVD may be exploited in such a way so as to obtain shorter pulses. The final duration of the pulse is determined by the interaction of SPM and GVD. This is usually achieved by including dispersive elements in the laser cavity which provide adjustable GVD of the opposite sign to the laser medium and other components. The prism is such a dispersive element. Brewster angled prism pair is inserted inside the oscillator cavity, to provide adjustable

intra cavity GVD. Specially designed dielectric mirrors are also used. Using prism pairs or optically designed dielectric mirrors (chirped mirrors) to control the net cavity GVD, brings about the generation of ultra short pulse. Once mode locking has been achieved, to obtain the ultimate bandwidth limited pulse duration, the GVD on each cavity roundtrip should be close to zero.

Chirped Pulse Amplification and dispersion control

Progress in ultrafast optics is dependent on the development of ways to characterize, measure, manipulate and manage dispersion and nonlinear interactions in the gain medium and other optical components. The means by which this can be accomplished in a laser oscillator is different from that in a laser amplifier. It is necessary to take into account the group velocity dispersion of the laser pulse as it traverses the amplification system. It is also imperative to measure and control the nonlinear optical effects that are bound to surface during this amplification process. Femto-second

laser pulses have very high peak powers and associated high electric fields and the peak power increases, even as the pulse amplifies and extracts a modest energy from the gain medium. This induces beam distortion and optical damage in the gain medium and the other optical components through which the beam propagates. Self focusing and SPM are responsible for these damages. For efficient extraction of energy from amplifiers, pulses should have fluences (pulse energy per unit area) close to the characteristic saturation fluence of the laser amplifier material, a requirement easily met by nanosecond pulse amplifiers, without the risk of inducing optical damage. Operation at those same fluences, with pulse duration in the femto-second range, is not possible without inducing self focusing and self phase modulation, leading ultimately to severe damage to the material or the gain medium. One method of overcoming such beam intensity limitations of ultra short pulse amplification, is to increase the amplifier medium cross-section or aperture to accommodate a beam size,

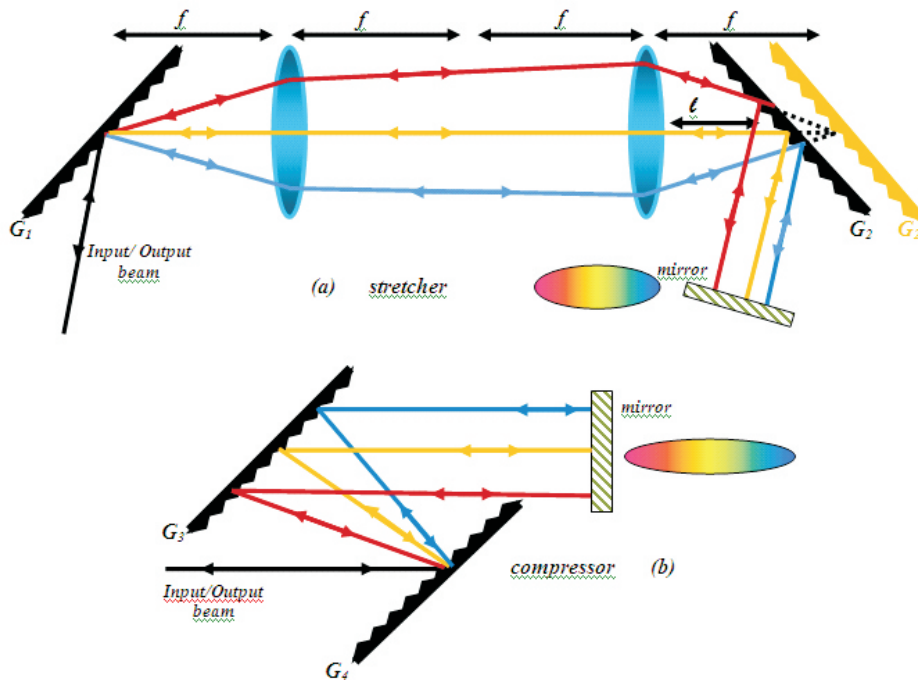


Fig.3. The schematic of the basic structure of a stretcher and compressor based on gratings. G_1 , G_2 , G_3 & G_4 are gratings with equal number of grooves or lines per mm. (a) The stretcher is a double pass stretcher. At the end of one pass through the stretcher the beam is collimated but spatially chirped (indicated by the elliptical beam on the mirror). At the end of the second pass through the stretcher the beam ideally becomes a circular cross sectioned beam with no spatial chirp, but chirped and stretched in time. (b) The input to the compressor is a stretched pulse. At the end of one pass through the compressor one gets a spatially chirped beam (elliptical beam on the mirror). After the second pass through the compressor the beam is ideally circular in cross-section, with no spatial chirp and compressed to an ultra short pulse.

arrangement. The fiber stretcher and diffraction grating compressor did not have their dispersive characteristics exactly complementary to each other. In other words the dispersive characteristics or the GVD did not match, giving rise to temporal side-lobes to the main pulse. The compressed pulse had a central high peak, which was accompanied with wings (or pedestal) on either side. The parameter that quantifies such a pulse, is the contrast ratio. Temporal contrast is defined as the ratio of the intensity of the main pulse to the intensity of the pedestal or sub-peak pulse. In high intensity laser plasma physics experiments, poor temporal contrast ratio caused by pre-pulses (or background pedestal or side lobes) can change the properties of target before the arrival of the main laser pulse.

It wasn't long, before a pulse stretcher, constructed with the help of a telescope of magnification one, placed between two anti-parallel configured gratings [4] was devised to obtain positive GVD. In place of the optical fiber stretcher a grating based stretcher was employed. This dispersive device had the exact same function as the parallel pair of grating compressor but with opposite sign. This was the compressor's exact conjugate. This means that, in theory a short pulse can be stretched to any pulse duration, and then recompressed to its exact original shape, without wings or pedestals. It was demonstrated that a stretching factor of 10^3 - 10^4 was achievable. Amplification in Nd:glass amplifiers and then compression led to the Table Top Terawatt (T^3) system or a high peak power system that fits into a small laboratory. In general for CPA systems, grating based stretcher/compressor design is used. The anti-parallel grating configuration as

that has been increased to proportionately reduced intensity. The required apertures would be impractically large and the laser system would be very inefficient. These are the limitations of direct amplification of ultra short pulses. In order to overcome this Donna Strickland and Gérard Mourou devised CPA, so that the short pulse can be manipulated in a controllable and reversible fashion. The amplifier medium never encounters a high peak power, high intensity short pulse. Therefore by stretching, amplifying and recompressing the ultra short pulse to nearly its original pulse duration, it is possible to circumvent the damage limitation of amplifiers and scale the ultra short pulse to very high peak powers.

The first CPA system used the positive GVD of a single mode fiber to

temporally spread the wavelength components of the ultra-short pulse. Donna Strickland and Gérard Mourou used a CW mode-locked, Nd:YAG oscillator [2] to generate 150ps pulses with $1.06\mu\text{m}$ as the centre wavelength of the spectrum. This was coupled into a 1.4km single mode fiber and the pulse that emerged was stretched to about 300ps. In the single mode fiber the red side of the infra-red wavelengths of the pulse travels faster than the blue side, resulting in positive GVD and therefore temporal stretching. It was then amplified in a Nd:glass regenerative amplifier before recompression in a pair of parallel diffraction gratings. A grating pair exhibits negative GVD [3] where the blue side of the spectrum travels faster than the red side. There was a problem in this kind of an

shown in **Fig.3 (a)** can generate even negative GVD, depending on the placement of the gratings. If grating G_2 is in the position shown in **Fig.3(a)** then the stretcher shows a $GVD > 0$. If G_2 is placed at the position marked with a 'yellow grating', then the $GVD = 0$. If G_2 is placed at a position beyond the 'yellow grating' marker, then the $GVD < 0$. An indigenously developed Nd:glass based CPA system at B.A.R.C [5][6] uses the pair of grating based stretcher/compressor design.

Many designs of the stretcher evolved over the years. The stretcher operates by introducing time delay for different spectral components of the ultra-short pulse. Therefore the output of the stretcher is a long chirped optical pulse. The dispersive element used could be either ruled gratings, holographic gratings, reflective or transmission type of gratings. For example in case of a Nd:glass based CPA system one can use holographic gratings with 1200 lines /mm. The unit magnification telescope in the stretcher [7] requires achromatic lenses. With this it is possible to stretch a 200fs optical pulse to 600ps and beyond. Some of the designs use all reflective optics [8] to provide high quality imaging at unity spatial and angular magnification. The stretchers need to have high spectral bandwidth and high fidelity. Retaining the entire band width is important because then the compressed pulse can be reduced temporally to the minimum possible. The performance of the stretcher is affected by the finite beam size, divergence, lateral walk-off of different spectral components and the aperture of the telescope. A well designed stretcher optimizes all these aspects of the beam along with the extent to which a temporal pulse can be stretched. The stretcher and the compressor design are generally in

the double pass mode. That means that the pulse encounters the gratings twice as schematically shown in **Fig.3**. This is because at the end of one pass the beam is spatially chirped. Only after the second pass, the spatial chirp becomes null. In this process of double passing, the temporal stretch (or compression) increases too.

The next step in the CPA system is the amplification. In the amplification process the regenerative amplifier is the first step in which a nano-Joule level energy pulse is amplified to an energy level of about a milli-Joule. After this the stretched pulse extracts energy from linear amplifiers, until the desired energy is reached. It is during this process that spectral narrowing occurs, the phenomenon that prevents the recompression, to revert the stretched pulse to its original temporal profile. The amplification in the gain media and also other optical components in the amplification system introduces, both amplitude and phase distortions, preventing the optimal recompression of the laser pulse. The compression grating pair, as a thumb rule, needs to have the same number of grooves as the stretcher gratings. Therefore, if gratings with 1200 lines/mm was used in the stretcher then the compressor gratings too should have 1200 lines/mm. The compression gratings have to be very large, because by this stage a very high energy level has been reached and peak power is also very high. This could damage the gratings if the beam does not have a large cross-section. Diffraction gratings are presently available with apertures of the order of one meter², allowing direct recompression to one Peta-Watt peak power or more. Stretching and recompression over many orders of magnitude in pulse duration, is a process that requires high accuracies in the design and

manufacturing of the optical components and in construction of the compressor. Many designs of the compressor have been tried out and suggested [9], mainly to obtain high peak powers in the final pulse and also to obtain high temporal contrast. In all CPA systems the non negligible higher order phase terms associated with the material dispersion in the components of the laser system limits the fidelity of recompression. The compressor design could compensate these phase terms to obtain a near clean temporal pulse.

High Peak Power Lasers and their applications.

Over the last three decades CPA has become the technique of choice for producing high peak power, ultra short pulses. High peak power lasers that fit into a small laboratory, can now reach focused intensities of the order of 10^{19} W/cm². Such lasers are widely being used in many types of laser plasma interaction experiments. Many of the "laser-matter-interaction" experiments depend on the high focused intensity, short pulse duration and a good pulse contrast ratio. For many experiments the required interactions of the main pulse with the target is strongly perturbed if there is a pre-pulse intensity on target. Therefore as the main pulse intensities are increased with improving system design so must the contrast ratio.

At modest intensity levels, pump-probe experiments for chemistry, biology and material science, has opened up the door for ultrafast processes, not known before. Many applications have been motivated primarily because ultrafast laser pulses can interact with materials very differently from long pulses, enabling high precision removal of very small amount of material without melting, a property very useful in material

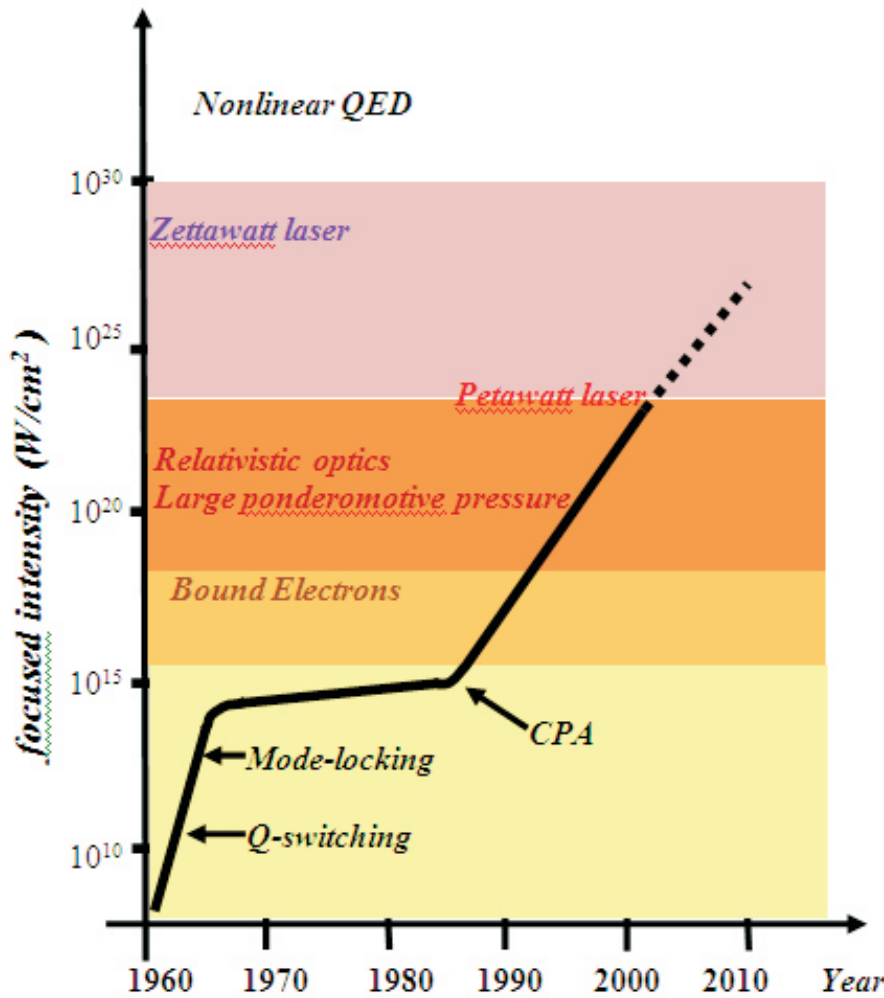


Fig.4. Laser intensity versus year with various physical thresholds. The achievable laser intensity shows a plateau for about 20 years due to limitations caused by nonlinear effects. The development of the laser systems over the years shows a turning point at 1985 with the discovery of the CPA.

processing. In fact when a material is cut or drilled with long pulsed lasers, the surrounding material shows the effect of heat transfer, micro-cracking, aftermath of a shock wave and zones of irregular material. While in case of an ultra-short pulsed laser, the material that is processed, gets a clean smooth finish, because none of the effects described, happens. There is only dense plasma in the vicinity of the laser impinging on the material leading to the smooth finish of the material. High precision material removal is very interesting in medical applications, where minimal damage to surrounding tissue is the need for most surgical procedures. Citing its mission to recognize inventions that benefit humankind, the Royal Swedish Academy has highlighted how Gérard Mourou and Donna

Strickland's work made possible production of surgical stents and the use of lasers (LASIK- Laser Assisted in-Situ Keratomileusis) to correct vision.

It is interesting to see the evolution of laser peak powers over the years. First the lasers were free running with the pulse durations in the few micro-second (μs) range and peak powers in the kilowatt range. Then a few years later, with the introduction of quality factor modulation in the laser cavity, the same energy could be packed into a nano-second (ns) time scale, to produce megawatt peak power. Mode-locking enabled the laser pulse duration to be reduced to the picoseconds level, pushing the peak powers to Giga-watt level. It means that intensities inside the laser

amplifier active medium could reach several Giga-watts per centimeter square (GW/cm^2). As described in the earlier sections, many nonlinearities show up at these intensities. A beam with a Gaussian radial intensity distribution, sees a larger index of refraction at the centre, than at the sides. All the optical elements in the path of the beam begin to behave as lenses, which unacceptably deform the beams wave-front quality. Therefore the only way to increase the peak power beyond the Giga-watt level was to increase the beam diameter and therefore the size of the gain medium and the size of all the other instruments. This not only increased the cost, but it was difficult to implement practically too. Although the pulse duration kept decreasing over the years, the intensity dependent non-linear effects kept the peak powers at a constant level, (Fig.4) for many years until CPA was invented. The years after the 1985 invention, saw a very quick rise in peak powers. Today it is possible to obtain powers in the Peta-watt range. Enormous intensities, of 10^{20} - 10^{22} W/cm^2 is made available on target. The field strength at these intensities (I) is of the order of a Tera-volt per cm, or hundred times the Coulomb field binding the ground state electron in the hydrogen atom. The light pressure ($P=I/c$) at these intensities is extreme (order of Giga-bar to tera-bar). The laser interaction with matter generates energetic electrons and ions. With laser intensities of 10^{18} - 10^{19} W/cm^2 it is possible to accelerate electrons to 80MeV-100MeV. These are nearly mono-energetic with an energy spread of a few percent. The electrons are accelerated by making them surf a laser driven plasma wave or the laser wake-field acceleration [10, 11] as it is popularly known. Analogous results

for ions too have been reached, with the production of quasi-mono-energetic protons. At intensities of 10^{21} W/cm² the electric fields become so high that the electrons accelerate to relativistic velocities. Subsequent to the acceleration of electrons up to relativistic energies, protons and ions are accelerated by well controlled mechanisms in a laser plasma acceleration setup. With a Peta-watt laser pulse, the emitted proton bunch was reproducibly observed with energies between 20MeV and 40MeV [12] and with a twenty five percent energy spread.

In many ways the physical environment of extreme electric fields, magnetic fields, pressure, temperature and acceleration can be found in stellar interiors. An astrophysical environment can be created in a laboratory! Scientific research in the field of Photo-transmutation of long lived nuclear waste is an ongoing endeavor, along with X-ray emission study and gamma-ray emission study. The exciting possibilities of using ultrahigh intensity lasers in a laboratory setting, opens the door to scientific research in areas of physical extreme. Even today there is still a challenge to make the pulse durations shorter and push the peak powers towards tens of Peta-watt and beyond.

Corresponding author and email:

Dr. Paramita Deb
(paramita@barc.gov.in)

References

1. A. Ashkin, "Acceleration and trapping of particles by Radiation Pressure", Physical Review Letters, Vol.24, No.4, 1970, 156.
2. Donna Strickland and Gerard Mourou, "Compression of Amplified Chirped optical pulses", Optics Comm., Vol.56, No.3, 1985, 219.
3. E. B. Treacy, "Optical pulse compression with diffraction gratings", IEEE. J. Quant. Electronics. QE-5, 1969, 454.
4. O.E. Martinez, "3000 Times Grating Compressor with a positive group velocity dispersion: Applications to fiber compensation in 1.3–1.6 μ m region", IEEE, J. Quant. Elect. QE-23, 1987, 59.
5. Paramita Deb, Kailash C. Gupta, Jayant K. Fuloria, L. Dhareshwar, V. Rajeshree and B.S. Narayan, "CPA Nd:glass laser system for intense laser matter interaction research", BARC Newsletter, February 2008.
6. Paramita Deb, Kailash C. Gupta and Jayant K. Fuloria, "Development of the chirped pulse amplification technique for high peak power production with Nd:glass laser system", BARC/E/022/2011.
7. Paramita Deb, L.J. Dhareshwar and B.K. Godwal, "Design Aspects of a grating pair stretcher / Compressor", Proceedings of Golden Jubilee DAE-BRNS National Laser Symposium 2003.
8. A. Offner, U.S. patent, 3748015, 1971.
9. Nandan Jha & Paramita Deb, "Temporal contrast improvement in chirped pulse amplification systems by a four grating compressor and by spectral modifications", Optik 125, 2014, 2261-2266.
10. T. Tajima and J.M. Dawson, "Laser Electron Accelerator", Physical Review Letters, 43, 1979, 267-270.
11. C.G.R. Geddes, Cs. Toth, J. van Tilborg, E. Esarey, C.B. Schroeder, D. Bruhwiler, C. Nieter, J. Cary and W.P. Leemans, "High-quality electron beams from a laser wakefield accelerator using plasma-channel guiding", Nature, 431, 2004, 538-541.
12. P. Hilz et al, "Isolated proton bunch acceleration by a Peta-watt laser pulse", Nature Communications, 2018, 9:423, 1-8.

Preparation of High Purity Boron by Molten Salt Electroextraction

Sanjib Majumdar, S. S. Molke, A. D. Sonawane, S. K. Gavai, R. Vanneldas,
P. S. Yadav, P. B. Shelke, Vivekanand Kain, Madangopal Krishnan
Materials Processing and Corrosion Engineering Division, Materials Group

Abstract

Molten salt electroextraction (refining) process was conducted to prepare elemental boron using the electrolyte KCl-KBF₄-KF and boron carbide (B₄C) as soluble anode. The reactor and the associated equipments for molten salt electrolysis were designed and fabricated in-house. The experiments were conducted using the indigenously made electrolytic cell at the temperature of 820°C with a varying time from 3 to 24 h by maintaining constant current. The cathode was removed after cooling and dipped in de-mineralised water for about 4-24 h. The deposited boron was scraped out of the cathode and further milled in planetary ball mill. The milled powder was leached, filtered and subsequently dried in vacuum. The morphology and composition of the electro-deposited boron was characterized using SEM, EDS and chemical analysis. High purity (97.7 ± 1.3%) boron was successfully electro-extracted.

Keywords: Molten salt electrolysis; Boron powder; Electroextraction; Boron carbide; Scanning electron microscopy

Introduction

Boron is a metalloid possessing attractive properties such as high melting point (~2076°C), low density (2.37 g/cm³), high hardness (9.5 in Mohs hardness scale), high neutron absorption cross section, and generates high exothermic heat in oxidizing reactions. Boron powder is used as a rocket fuel igniter and in pyrotechnic flares. Boron powder is also extensively used in pyro-chemical formulations for the preparation of a wide range of military explosives [1]. Enriched boron carbide (B₄C) pellets prepared by solid state reaction between boron and carbon and subsequent hot pressing, are used in control and diverse safety rods for Prototype Fast Breeder Reactor (PFBR). Elemental boron is used as deoxidizer, degasifier etc. in various metallurgical applications.

Different methods are in practice to produce elemental boron such as (1) molten salt electrowinning or electroextraction using molten chloride or fluoride salts and borates or fluoroborates as boron source [2];

(2) metallothermic reduction of B₂O₃ using the reducing agents like Mg, Li, Na, K, Al [3]; (3) hydrogen reduction of boron halides like BCl₃ and BBr₃ [4]; and (4) thermal deposition [5]. The molten salt electrolysis is considered as the most promising method for preparing elemental boron due to the simpler process technology, and high purity product obtained at a comparatively low cost [6].

Miller [7] reported the electrodeposition of boron from a melt containing KCl (70 wt. %), KF (12 wt. %) and KBF₄ (17.8 wt. %) in the temperature range 1023–1073 K. Subsequently, the electrowinning of B was carried out in this laboratory [1] using the Miller's salt composition at 1073°C. The earlier authors [1] have also reported the electroextraction of boron from B₄C in NaCl-KCl-KBF₄ bath. Production of elemental enriched boron (~65% ¹⁰B) is in practice in Heavy Water Plant, Manuguru, using the electrowinning technology demonstrated at Indira Gandhi Centre for Atomic Research (IGCAR), Kalpakkam, India [8, 9]. In the present work, a demonstration facility has been further re-designed

and fabricated for carrying out the electroextraction of pure boron from B₄C using KCl-KBF₄-KF melt bath.

Method

Laboratory grade (LR) KCl, KF and KBF₄ were used in appropriate ratios, and the salt mixture was made using a tumbler mixer. Before mixing, the salts were individually dried between 250-400°C inside a vacuum furnace maintaining a vacuum level of about 10⁻¹-10⁻² mbar. The salt powder mixture was subsequently charged inside the graphite crucible, which was placed inside a cylindrical inconel retort. The overall outlook (set up) of the electrolytic cell is presented in Fig. 1(a). A properly designed inconel retort (Fig. 1b) is placed inside a pit type kanthal wire heated resistance furnace. The electrolytic cell was designed and fabricated in-house. Boron carbide (B₄C) chunks were used as anode feed. The B₄C chunks were placed around the inner periphery of the graphite crucible, and the chunks were separated from the salt mixture by a perforated graphite crucible which was subsequently filled with the salt mixture. The electrical connection of

the anode was provided to the graphite crucible through the inconel retort. The cathode plate made of mild steel (MS) was fixed on a stainless steel rod and inserted through the centre of the top flange of the retort. The connection of the cathode was given from a DC power supply to the top end of the SS rod (see Fig. 1b). The cathode plate was placed about 20 mm above the salt powder bed at room temperature. The temperature of the pit furnace was increased to 400°C by maintaining a vacuum inside the retort and held for about 2 h. Subsequent heating to 820°C was carried out in argon flow. The cathode plate was pushed into the molten salt when the temperature reached at about 750°C. Initially, a pre-electrolysis run was conducted by applying a potential of about 1 V maintaining the cell current at 8 A for about 3h. The actual electro-extraction experiments were carried out at 820°C with varying cell voltage: 2 – 2.5 V, current: 20 – 22 A, and time: 3 – 24 h. After cooling, the cathode was removed from the electrolytic cell and kept inside demineralised water for 4 – 24 h. The deposited material was removed from the MS cathode, and after filtering out from the water, it was ground using motor-pestle and subsequent planetary ball milling. The milled powder was leached with dilute HCl water solution. After filtration and washing, the powder was dried in vacuum and the final product (Boron) was obtained. The detailed characterization of the dry powder was carried out using chemical analysis, XRD, SEM-EDS etc.

Results and Discussion

a) Electro-extracted Boron

Fig. 2(a) shows the appearance of the as-deposited product obtained after conducting the molten salt electroextraction process for 7 h at



Fig. 1: (a) Molten salt electrolysis set up, and (b) Top part of the retort of the electrolytic cell

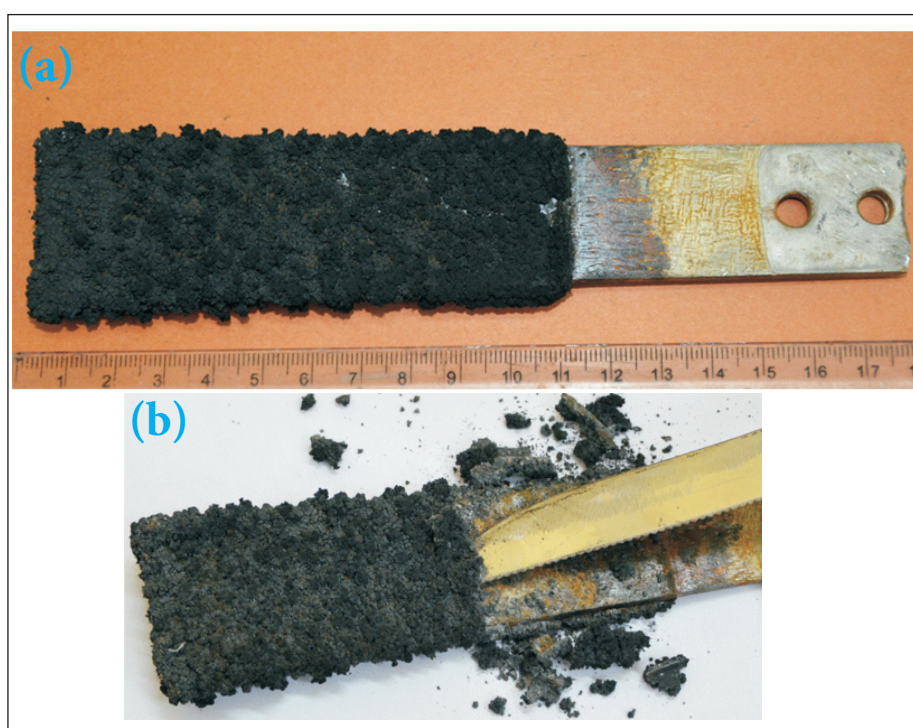


Fig. 2: Outlook of (a) the electro-deposited boron on MS plate, and (b) removal of boron from MS plate using knife edge

Table 1 Chemical analysis data of the electro-extracted product

Element(s)	B	O	C	F
Wt.%	97.7 ± 1.3	0.25	0.1	46 ppm

820°C in argon atmosphere. Gray to dark gray coloured deposits were obtained on the mild steel cathode. The deposits showed the tendencies of forming agglomerates when dried in contact with the MS plate. The deposits were removed from the MS plate using the knife edge (Fig. 2b). Presence of salt was observed at the

interface between the deposit and MS plate. The salt was further removed by grinding and washing the powder in subsequent stages of treatment. The detailed chemical analysis report of the electrodeposited powder is presented in Table 1. The boron content in the powder was detected to be about 97.7±1.3%. The morphology

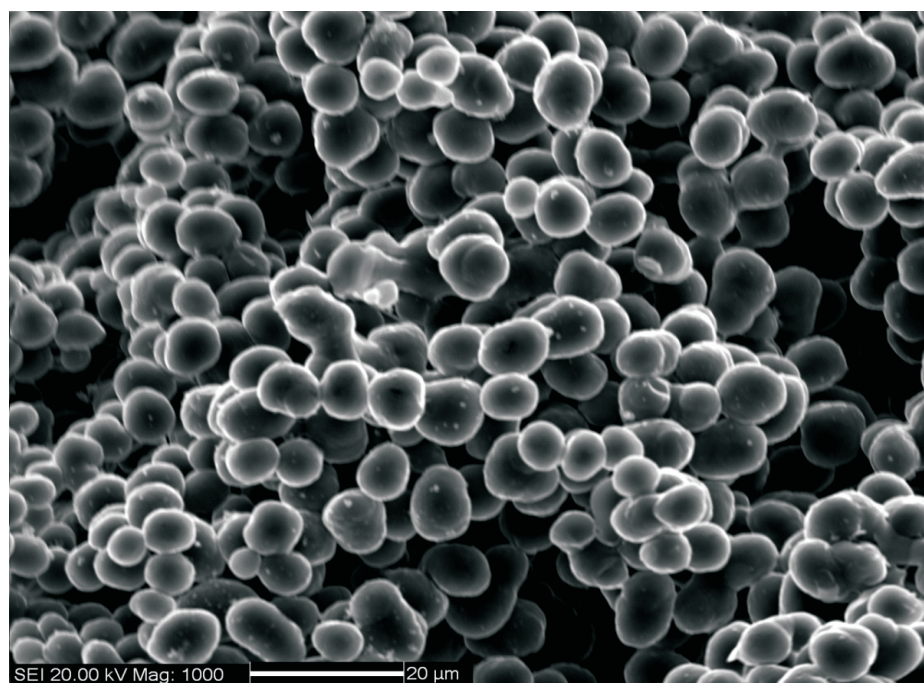


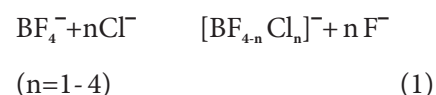
Fig. 3: SEM image showing the surface morphology of the as-deposited boron

of the electro-extracted boron observed under SEM is presented in Fig.3. Spherical or round-type of particles of size ranging in 6-9 µm was developed during electro-deposition. At this stage, the boron powder particles were present in agglomerated condition. EDS analysis carried out on the individual particle (Fig. 4a and 4b) revealed the presence of pure (99.9%) Boron. The as-deposited boron was further ground using planetary ball milling, leached with dilute HCl solution, filtered, vacuum dried, and finally, pure boron powder of different size ranges were produced.

b) Molten salt electroextraction: Process Optimization

The major anions present in the molten salt of KCl-KBF₄-KF are Cl⁻, BF₄⁻ and F⁻. BF₄⁻ anions are relatively larger in size, and therefore, different types of interactions are possible amongst the anions depending upon the variation of the concentration of individual salts.

The eutectic crystallization temperature (or melting point) of the salt mixture varies between 425°C to 650°C [10] from a salt composition of 0.04KCl-0.80KBF₄-0.16KF to 0.64KCl-0.20KBF₄-0.16KF. Therefore, the melting temperature increases with increase in concentration of KCl. Amongst the various reactions, the most probable interaction of three anions are reported to be the exchange of the fluoride atoms, in the BF₄⁻ tetrahedron with chloride ions according to the following reaction.



The probable reactions occurred during molten salt electroextraction process at the cathode and the anodes are furnished below.

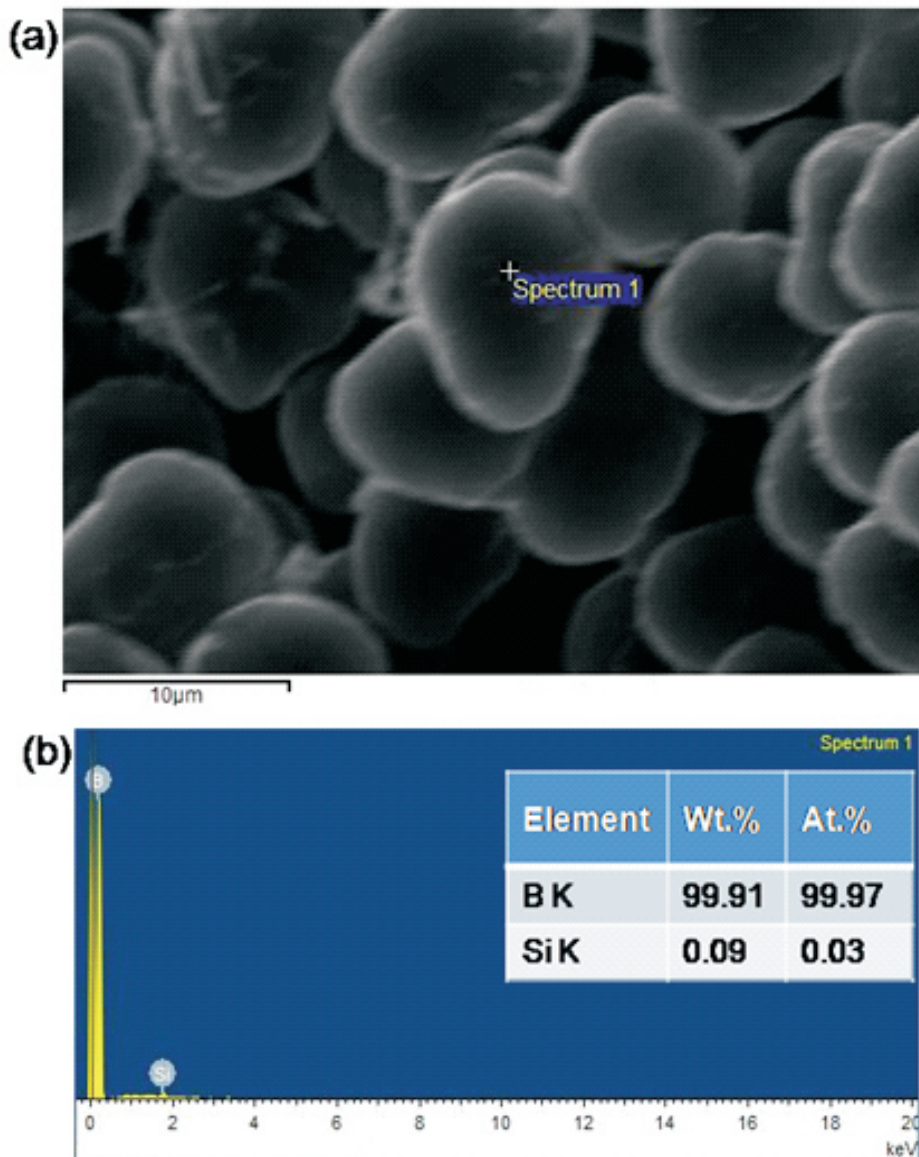
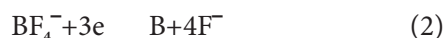
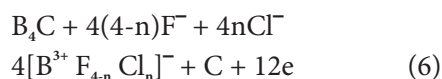


Fig. 4: (a) SEM image showing individual boron powder, and (b) EDS X-ray spectrum confirming presence of boron

Cathode:



Anode:



With the application of initial voltage (0.5 - 1 V) the salts get decomposed and the deposition of boron (B) starts at the cathode as per the reactions (2) and (3). Evolution of fluorine (F₂) and chlorine (Cl₂) gases occur simultaneously at the anode according to the reactions (4) and (5). With increasing time, B₄C dissociates from the anode as B³⁺ by forming [BF_{4-n}Cl_n]⁻ ions as per reaction (6), and these ions gradually move into the molten salt. Therefore, during the course of the molten salt electroextraction process the reactions (3) and (6) dominate. The concentration of boron ion in the salt remains constant due to the continuous supply of boron from the anode feed i.e. boron carbide. Therefore, the evolution of chlorine and fluorine gases becomes negligible as the electroextraction process progresses. The concentration of carbon would increase near the anode with increasing time of operation of the electrolytic cell. Fig. 5 shows the Evs. I plot obtained during electrolysis process. It can be observed from Fig. 5 that with increasing potential towards positive values, the current increases continuously. This phenomenon is typically the same as those resulting from the decomposition of a solvent or electrolyte and/or dissolution of electrode, which defines the 'potential range' in cyclic voltammetry [11]. Hence, decomposition of salt in the electrolyte, dissolution of B₄C at

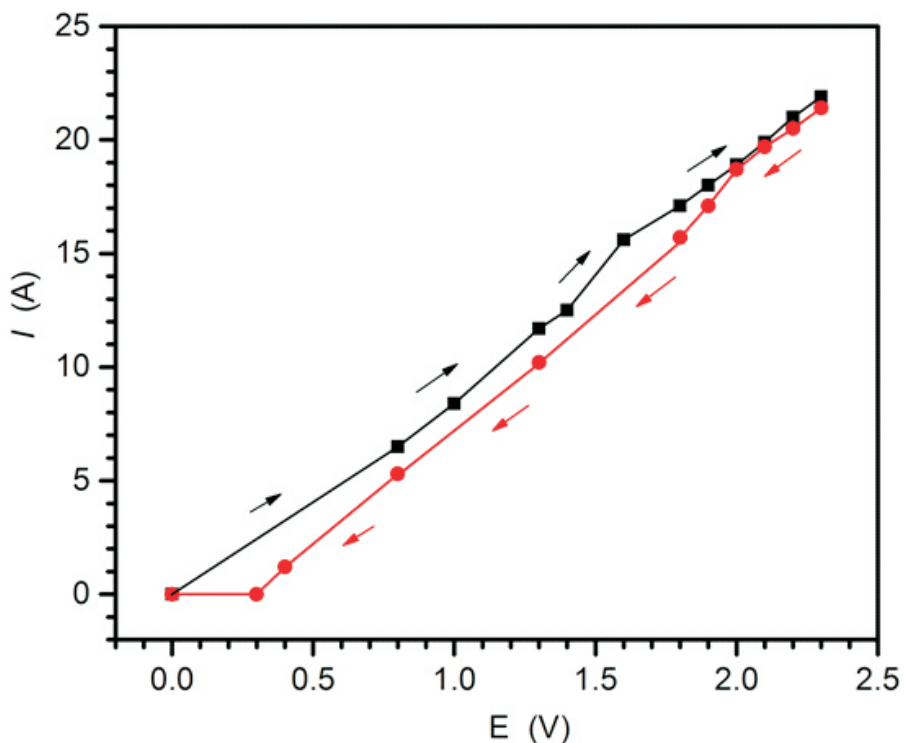


Fig. 5: Current vs voltage plot obtained during molten salt electrolysis

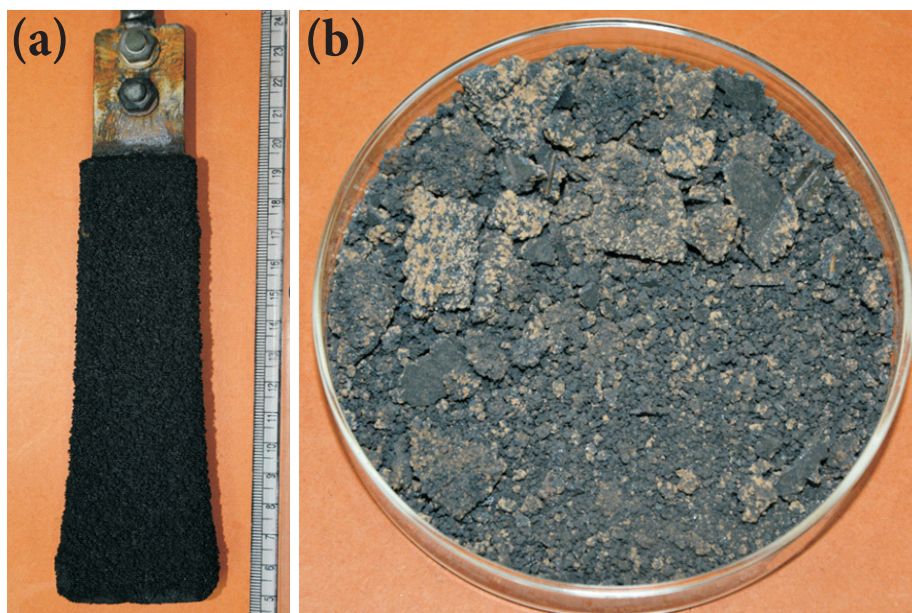


Fig. 6: Outlook of (a) electrodeposited boron on cathode plate, and (b) Boron (~55g) after removal from cathode

anode and deposition of B at cathode dictate the overall electroextraction process. The temperature of the process was kept at 820°C to increase the boron deposition (reaction) rate by maintaining the current at about 22 A. In general, the rate of deposition increases with increasing temperature and increasing voltage. The electrolytic cell was operated for different time intervals from 3 to 24 h. Fig.6(a) shows the outlook of the

boron deposited MS electrode obtained after 12 h of cell operation. About 55g of boron obtained from the cathode (in 12 h) is presented in Fig. 6(b). 150 g of boron powder was obtained after operating the cell for 24h. Further optimization of the process with respect to increase in cathode surface area, cell current and temperature are in the scope of the future work.

Conclusions

High purity boron was produced by molten (fused) salt electroextraction process using B_4C chunks at anode and $KCl-KBF_4-KF$ salt as electrolyte. The as-deposited boron showed spherical morphology, and the fine size boron powder could be produced by performing further grinding and milling of the electrodeposited product. The produced boron powder could be used in different application areas of nuclear industry, defence and space. The electrolytic cell was designed and fabricated indigenously, and the parameters of the electroextraction process were optimized. This technology is now available from BARC for large scale production of pure boron powder.

Corresponding author and email:
Dr. Sanjib Majumdar
(sanjib@barc.gov.in)

Acknowledgements

Authors thank Shri S. B. Chavan and Shri S. Behera of High Temperature Materials Development Section, MP&CED, for their technical assistance during experimental campaign. The support from Analytical Chemistry Division in providing detailed chemical analysis report of the electrodeposited product is gratefully acknowledged.

References

1. K. U. Nair, D. K. Bose, C. K. Gupta, Miner. Proc. Extrac. Metall. Rev. 9, 1992, 283–291.
2. H. S. Cooper, U.S. Pat., 2, 572, 249, 1951.
3. N. N. Greenwood, A. Earnshaw, Chemistry of the elements, Butterworth-Heinemann, 1998.
4. D. T. Hurd, J. Am. Chem. Soc. 71 1949, 20–22.
5. D. K. Das, K. Kumar, Thin Solid Films 83, 1981, 53–60.
6. Qian Wang, Yan Li Wang, Hui Jun Liu, Chao Liu Zeng, RSC Adv. 6, 2016, 55953–55960.
7. G.T. Miller, J. Electrochem. Soc. 106, 1959, 815–819.
8. Rahul Pal, K. Ananthasivan, S. Anthonysamy, V. Ganesan, Electrochim. Acta 61, 2012, 165–172.
9. Ashish Jaina, S. Anthonysamy, K. Ananthasivan, R. Ranganathan, Vinit Mittal, S.V. Narasimhan, P. R. Vasudeva Rao, Mater. Character. 59, 2008, 890–900.
10. O. Patarak, V. Danek, Chem. Papers 46(2), 1992, 91–94.
11. George Zheng Chen, Derek J. Fray, Tom W. Farthing, Nature 407, 2000, 361–364.

Synthesis and Evaluation of Polyphenolic Malabaricones for their Anti-cancer Potential

¹Mrityunjay Tyagi, ¹Kshma Kundu, ¹Ajay Kumar Bauri, ^{1,2}Birija Sankar Patro and ^{1,2}Sandip Kumar Nayak

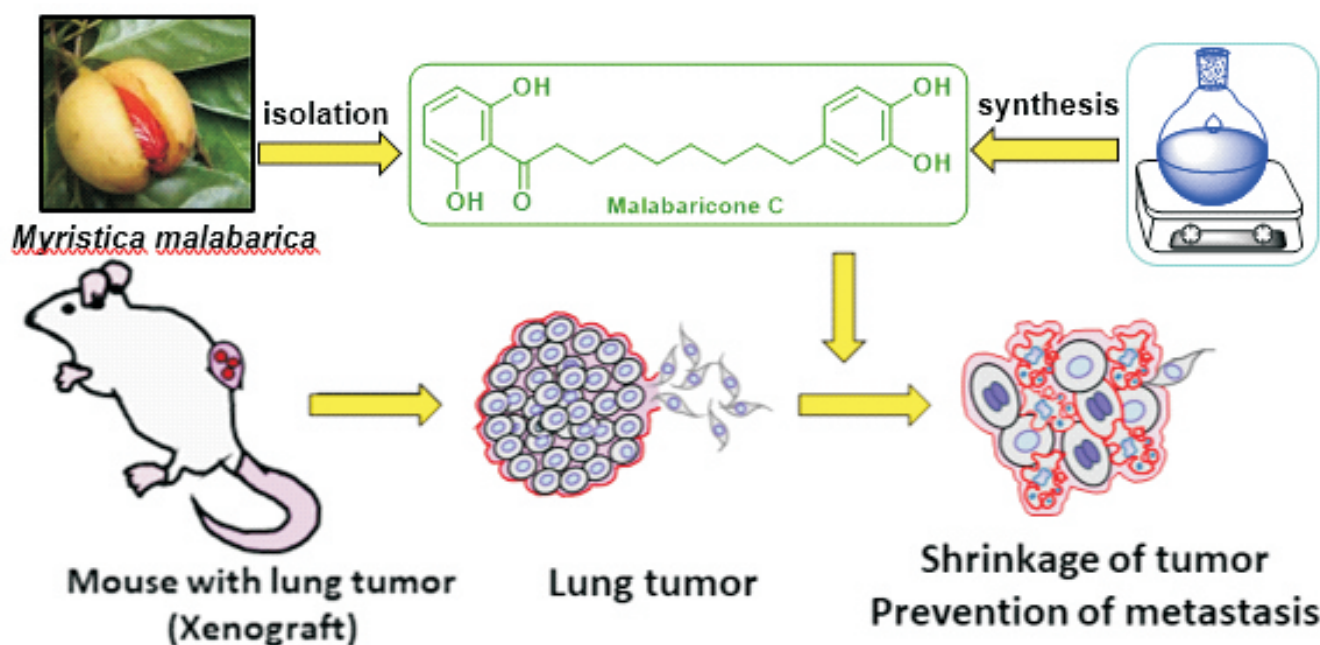
¹Bio-Organic Division, Bhabha Atomic Research Centre, Mumbai-40085

²Homi Bhabha National Institute, Training School Complex, Anushaktinagar, Mumbai-400094

Abstract

Cancer is one of the leading causes of deaths all over the world. The search for the novel drugs is essential for chemotherapy, due to inherent or acquired resistance in cancer cells against conventional chemotherapy. Dysregulation in apoptotic pathways, improved DNA repair, drug transport and detoxification are considered to be the major causes of drug resistance. There is a burgeoning interest in small natural organic molecules, capable of switching their redox status, as these can often cleave DNA and/or target mitochondria, and hence can be used as anti-cancer agents. To this end, this review describes the discovery of an important polyphenolic viz. malabaricone C (Mal C), which was isolated from fruit rind of rampatri spice, possessing impressive anti-cancer properties in vitro and in vivo tumor models. Mal C shows higher therapeutic efficacy than curcumin and resveratrol against multiple cancer cells. This review also highlights synthesis and mechanistic evaluation of mal C and its analogue for their anticancer potential.

Keywords: Myristica malabarica, Malabaricones, Cancer therapy, Redox regulation, Mitochondrial dysfunction



Introduction

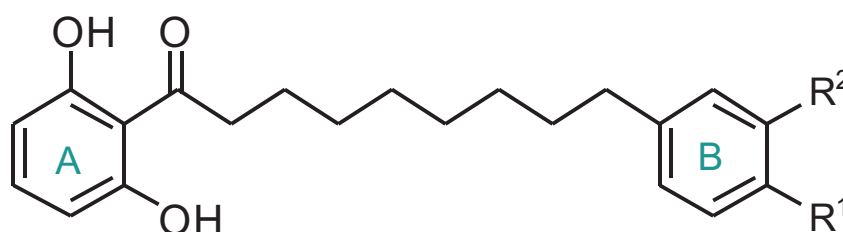
Cancer is one of the leading causes of mortality in developing countries with lung and breast cancer contributing maximum cancer related mortalities in men and women, respectively [1]. Lungs and breast cancer contributes to 5.9% and 14% of new cases of cancers per year in India, and

accounts for 19% of cancer related deaths worldwide [1]. Apart from primary lung cancers, lungs are the second most common sites for metastatic spread [2]. In particular, the aggressive and highly metastatic late stage melanoma is well-known to induce secondary lung cancers. The 5-year survival rate is less than 15% in patients with metastatic disease and an approximately one-third of all

melanoma patients experience disease recurrence [3]. Various chemotherapeutic agents are being exploited for management of lung cancer, breast cancer and metastasis. However, systemic hemato-and-neuro-toxicity/side-effect and cancer recurrence because of inherent or acquired resistance remain major issues in cancer therapy [4]. Drugs that can modulate the actions of

multiple targets may reduce/overcome the chances of drug resistance and recurrence in cancer therapy.

Current epidemiological evidences show a strong influence of specific diet on cancer prevention. Extensive work is also being pursued to identify compounds from dietary and medicinal plants and other natural resources, as these are popularly believed to be non-toxic to humans [5]. Also, an approximately 50% of the internationally approved chemotherapeutic drugs are derived from natural products [6]. Spices are present in most of our daily diets, and consumption of spice rich food has been found to play an important role in suppressing the transformative, hyper-proliferative and inflammatory processes that initiate carcinogenesis [7]. The fruit rind of the plant *Myristica malabarica* (Myristicaceae) (popularly known as rampatri, Bombay mace, or false nutmeg) is used as an exotic spice in various Indian cuisines. This is credited with hepatoprotective, anticarcinogenic, and antithrombotic properties and is found as a constituent in many Ayurvedic preparations such as pasupasi. Several herbal formulations containing *M. malabarica* are also claimed to possess antitumor effect [8]. However, most of the medicinal attributes of the spice have not been substantiated adequately. Earlier, we have found that amongst the four malabaricones A–D (designated as mal A–D), isolated from its extract, mal B and mal C possess superior antioxidant [8], anti-inflammatory [9], anti-ulcer [10, 11] and cardio-protective properties [12]. The chemical structures of mal A–D are shown in Fig. 1. For last several years, extensive investigation was carried out to identify the active constituents and their mode of action in killing lungs and breast cancer cells.



Malabaricone A (1a): $R^1 = R^2 = H$

Malabaricone B (1b): $R^1 = OH; R^2 = H$

Malabaricone C (1c): $R^1 = R^2 = OH$

Malabaricone D (1d): $R^1, R^2 = O-CH_2-O$

Fig.1. Chemical structures of malabaricones (A-D) isolated from methanolic extract of dried fruit rind of rampatri.

Mode of action of malabaricones against breast cancer cells

There is a burgeoning interest in finding natural redox active molecules, which can often cleave DNA, and hence can be used as anti-cancer agents. Although, the redox potentials of a variety of metal ions have been exploited for the development of DNA cleaving agents, the organic compounds possibly play more important roles in this regard, as they provide a multitude of binding interactions with the target DNA, while ensuring the required electron transfer via their intrinsic chemical, electrochemical and photochemical properties [15]. Initially, we focused on assessing the potential of the malabaricones as the DNA cleaving agents, and whether this confers them with anti-cancer properties. The nuclease activities of the malabaricones (A-D) have been studied so as to establish a structure–activity correlation and deduce the mechanistic pathway of the process [15]. The inactivity of mal A and mal D revealed that the resorcinol moiety, present in the malabaricones did not contribute to the nuclease activity. Amongst the test compounds, mal C containing a B-ring catechol moiety showed

significantly better Cu(II)-dependent nuclease activity than the partially methylated catechol derivative, mal B and curcumin (Fig. 2A). Mechanistically, mal C was found to bind efficiently with Cu(II) and DNA to facilitate the DNA nicking via a site-specifically generated Cu(II)-peroxo complex (Fig. 2B) [15]. Consistent with its Cu(II)-dependent nuclease property, mal C showed better cytotoxicity (IC_{50} : $5.26 \pm 1.2 \mu M$) than curcumin (IC_{50} : $24.46 \pm 3.3 \mu M$) against the MCF-7 human breast cancer cell line. The mal C-induced killing of the MCF-7 cells followed an apoptotic pathway involving oxidative damage to the cellular DNA (Fig. 2C) [15]. The cellular DNA fragmentation by mal C that involves mobilization of intra-cellular and extra-cellular Cu(II), could be one of the mechanisms involved in its chemopreventive property.

Further, our study revealed mal C induced mitochondrial damage. This was assessed by fluorescence microscopy and flow cytometric analyses of the JC-1- stained cells (Fig. 2 C&D) [16]. Besides, mal C treatment led to a significant increase in lysosomal membrane permeabilization (LMP), along with the release of cathepsin B, as well as

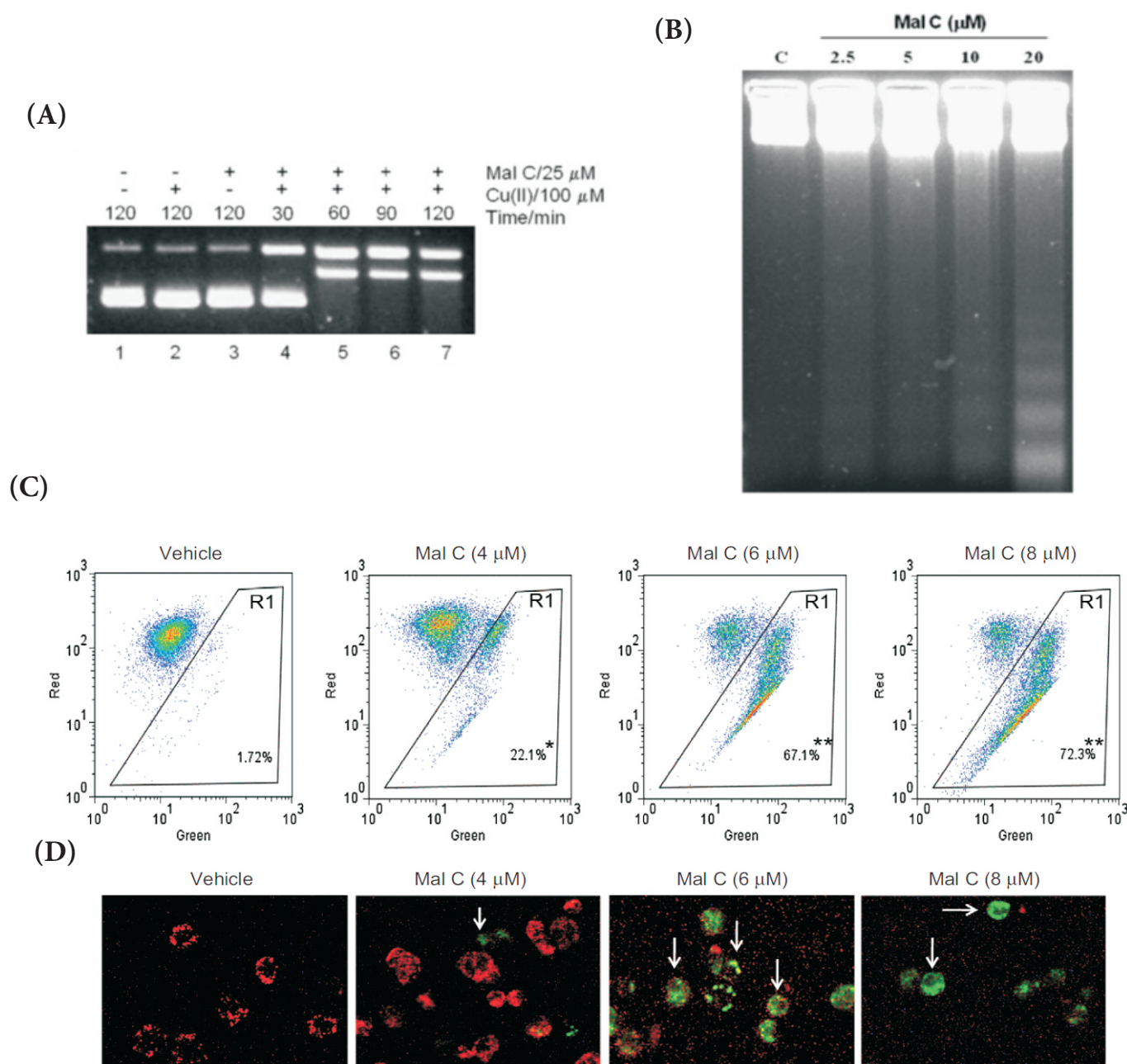


Fig. 2. (A) Copper ion-dependent nuclease activity of mal C. (B) Mal C induced cytotoxicity is mediated through internucleosomal DNA fragmentations. Mal C permeabilizes mitochondrial membrane in breast cancer cells. Loss of mitochondrial membrane potential (MMP), assessed by (C) flow cytometry and (D) fluorescence microscopy. The cells were incubated for 6 h with mal C (0, 4, 6, and 8 μ M), stained with JC-1 for 15 min, and MMP loss quantified by flow cytometry from the increased green fluorescent cells.

BID-cleavage and its translocation to mitochondria. Mal C induced LMP occurs prior to mitochondrial dysfunction in breast cancer cells. This suggested that cytotoxicity of mal C against human human breast cancer cells may proceed through LMP as the initial event that triggered a caspase-independent, but cathepsin B and t-BID-dependent intrinsic mitochondrial apoptotic pathway. Moreover, a significant accumulation of cells in the S or G2-M phases along

with upregulation of the cyclins E and A due to mal C exposure promises it to be a potential anti-cancer agent [16].

Malabaricone C induced robust killing of lung carcinoma cells through a DNA damage dependent activation of CHK1-p38 MAPK pathway.

In order to evaluate the efficacy of malabaricones against lung carcinoma, the cytotoxic potential of

malabaricones were tested against a panel of lung carcinoma (A549, NCI-H23, and NCI-H460) cells. Our results showed that mal A-D and curcumin induced cytotoxicity in A549 lung carcinoma, with IC50 values of $19.2 \pm 4.2 \mu$ M (mal A), $8.4 \pm 2.5 \mu$ M (mal B), $7.0 \pm 1.8 \mu$ M (mal C), $20.3 \pm 5.1 \mu$ M (mal D) and $41.7 \pm 6.2 \mu$ M (curcumin). Further, the mal C also found to induce cytotoxicity with similar IC50 values in several other lung cancer cells e.g., IC50 of 7.7 ± 2.1

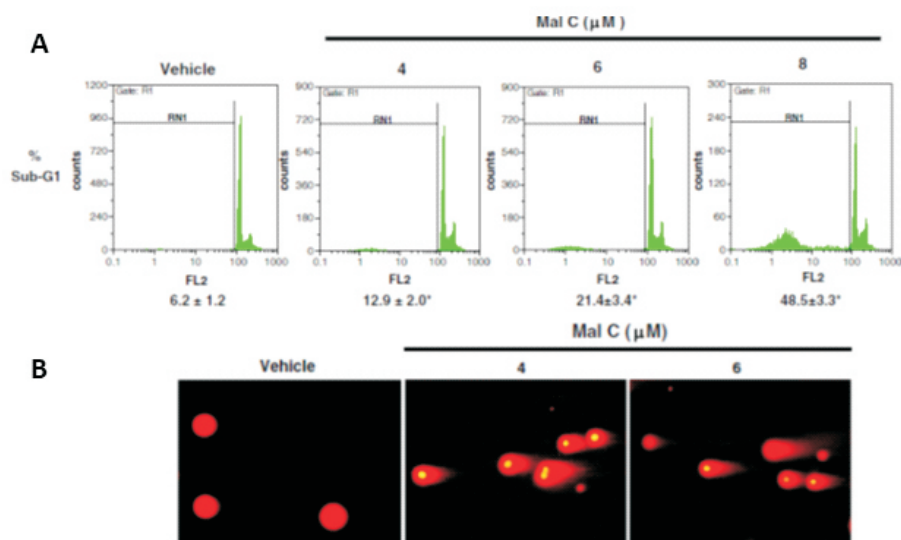


Fig. 3. Mal C treatment induces (A) apoptotic cell death (B) DNA double strand breaks (DSBs) in A549 lung carcinoma. * $p < 0.01$ compared to vehicle control.

simultaneous enhancement in apoptosis of breast carcinoma in patients. However, it is not yet precisely known how thiol antioxidants enhance killing of cancer cells, or any putative agent can tweak the cancer cells survival program in NAC/glutathione (GSH)-assisted manner to make cancer cells vulnerable to death. To this end, we showed that a dietary compound, malabaricone C (mal C), generated copious amounts of reactive oxygen species (ROS) and also reduced the GSH level in lung cancer cells (Fig. 4A & B).

Paradoxically, although antioxidants supplementation reduced mal C-induced ROS, thiol-antioxidants (NAC/GSH) restored intracellular

μM for NCI-H460, $9.9 \pm 2.7 \mu\text{M}$ for NCI-H23, and $12.4 \pm 3.4 \mu\text{M}$ for NCI-H522 cells [17].

Mechanistically, our detailed investigation showed that mal C mediates apoptosis in multiple lung cancer cells, which is primarily associated with its ability to induce DNA double strand breaks (DSBs) (Fig. 3A&B) [17]. Subsequently, DSBs cause ATM/ATR-mediated activation of CHK1. Further, CHK1 induced rapid phosphorylation of p38-MAPK, which paralleled with mitochondrial dysfunctions in terms of imbalance in BAX/BCL2 expression, cytochrome-C release [17]. This conclusion is based on the fact that mitochondria depleted and p38-MAPK inhibited lung cancer cells are resistant while BCL2 knock-down cancer cells show higher sensitivity to mal C treatment [17]. Together, mal C shows an impressive anti-cancer efficacy against human lung carcinoma cells.

Augmentation of therapeutic potential of malabaricone C by using N-acetyl cysteine as thiol antioxidant

Recently, targeting drugs to redox homeostasis of the cancer cells is considered as one of the key strategy for cancer therapy. Recent clinical

studies showed that N-acetyl cysteine (NAC) treatment significantly decreased the metabolic heterogeneity and reduced Ki67 (a proliferation marker) with

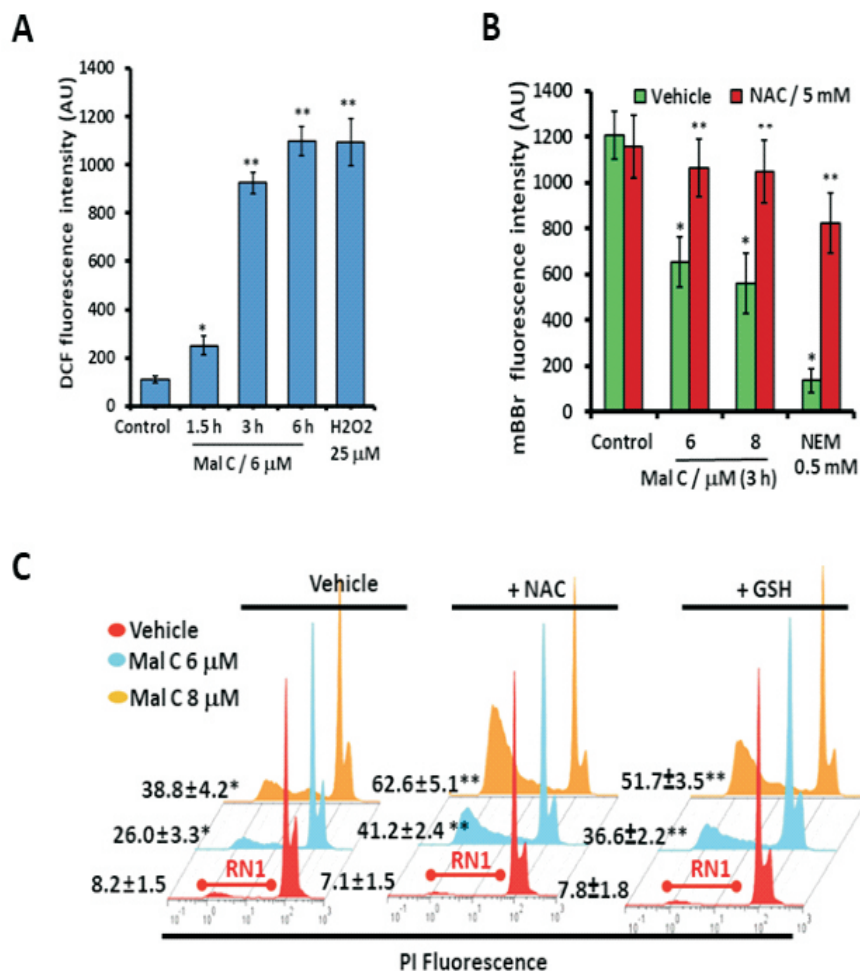


Fig. 4. Mal C treatment induces (A) ROS generation and (B) depletion of glutathione in cancer cells. (C) NAC or GSH antioxidant treatment enhances mal C mediated death process in A549 lung carcinoma cells. * $p < 0.01$, ** $p < 0.001$ compared to respective control in A, * $p < 0.01$ compared to control, ** $p < 0.01$ compared to respective mal C or NEM treatment in B and C.

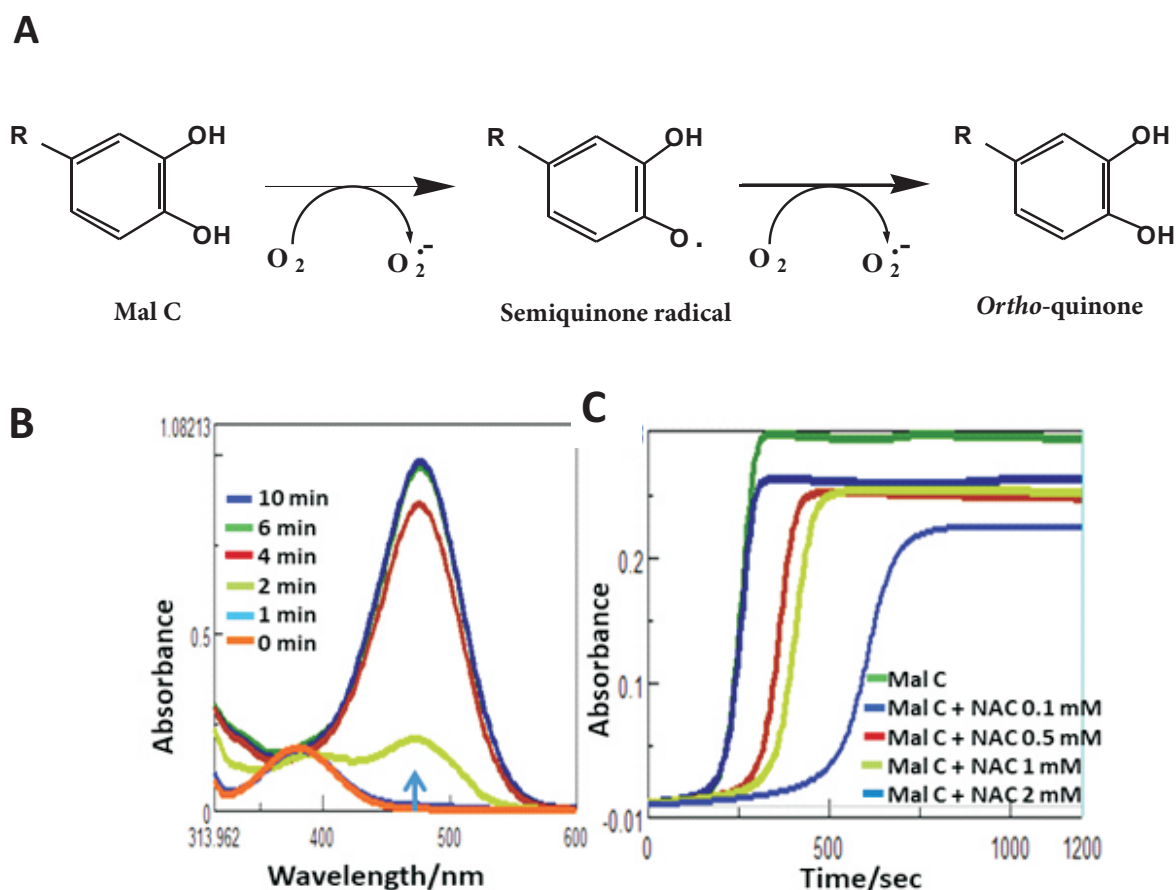


Fig. 5. (A) Schematic representation for autoxidation of mal C and generation of quinone forms and ROS. (B) Incubation of mal C generates quinone form (480 nm) in a time dependent manner. (C) Oxidation of mal C to its quinone form was delayed and reduced by thiol antioxidants.

GSH level but enhanced DNA DSBs and apoptotic cell death induced by mal C (Fig. 4 B & C). Mechanistically, our results unraveled two tightly coupled biochemical mechanisms attributing this sensitization process by thiol antioxidants. Firstly, it was anticipated that during $O_2^{\cdot-}$ radicals generation by mal C [25], its easily oxidizable catechol function will be converted to the corresponding ortho-quinone moiety (Fig. 5A). To this end, our results showed that the absorption spectra of mal C in culture media is shifted to progressive emergence of the quinone absorption peak at 480 nm, with simultaneous depletion of the mal C absorption at 373 nm (Fig. 5B). Co-incubation with NAC delayed the conversion, and the effect of NAC was concentration dependent. Moreover, the peak quinone levels in presence of NAC were much less vis-à-vis mal C incubation only (Fig. 6C). Together,

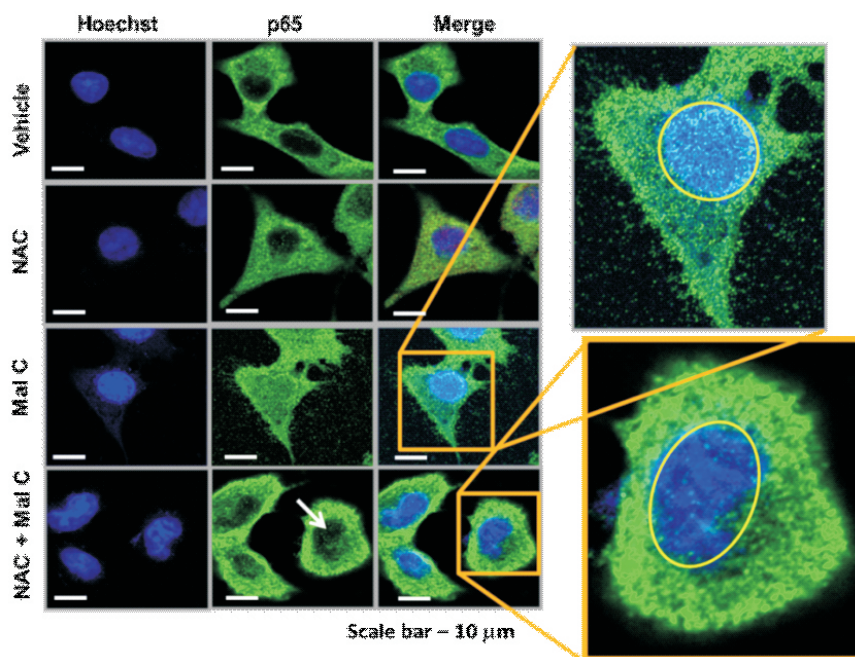


Fig. 6. Mal C treatment, in A549 lung carcinoma, enhances sequestration of p65 to nucleus. Mal C mediated nuclear sequestration of p65 protein was abrogated by NAC antioxidant.

our results showed that thiol antioxidants enable the “catechol-quinone redox cycle” of mal C and ameliorate ROS generation and bio-molecular damage (DNA and

protein). Secondly, thiol antioxidants cause rapid glutathionylation of transcription factors [p53, p65 (NF-κB) etc.], oxidized by mal C, and abrogates their nuclear sequestration

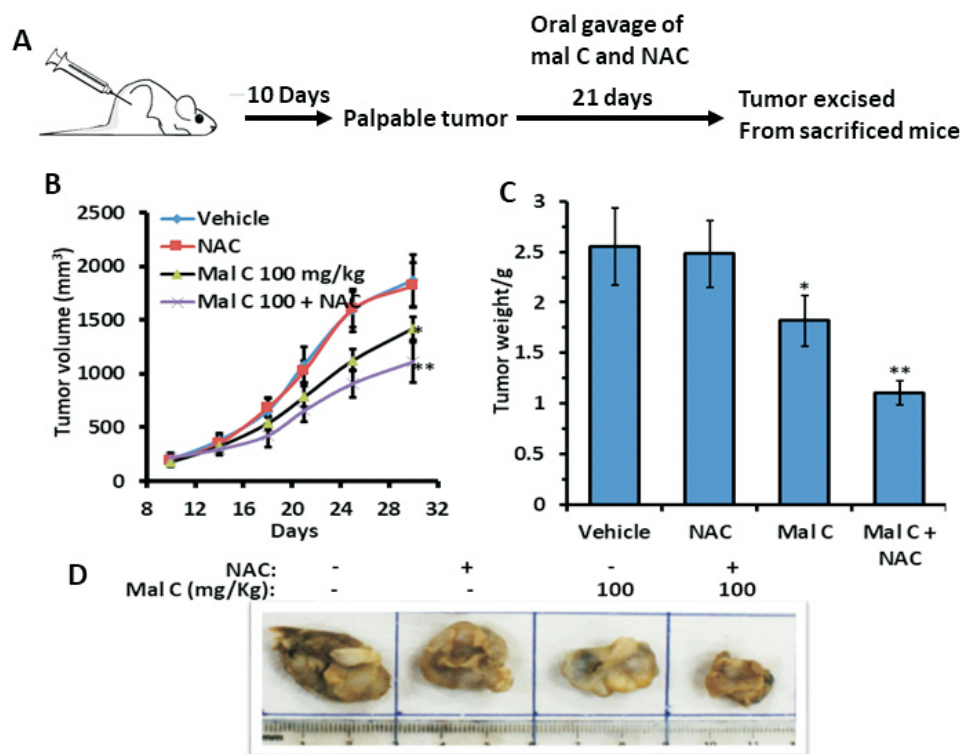


Fig. 7. Therapeutic efficacy of mal C alone or in combination with NAC in human lung tumor xenograft model. (A) Schematic representation of mal C and NAC treatment in tumor bearing mice model. (B-D) Oral gavage of mal C alone or in combination with NAC antioxidants significantly reduces lung tumor burden in mice. * $p < 0.05$, ** $p < 0.01$ compared to respective control

reduction in both these parameters. During treatment with mal C or NAC, either alone or in combination, there was no evidence of severe loss in body weight indicating that the combination was well tolerated. All these data support a potential use of mal C alone or in combination with NAC (thiol antioxidants) in the management of lung and melanoma tumors. Mal C is abundant in rampatri, which is extensively consumed in the eastern world without any side effect. Earlier, we found that mal C is non-toxic to mice, even at an appreciably high dose (500 mg/kg). Considering this encouraging findings, mal C appears to be a potent anti-cancer drug.

Gram scale syntheses of malabaricones B and C

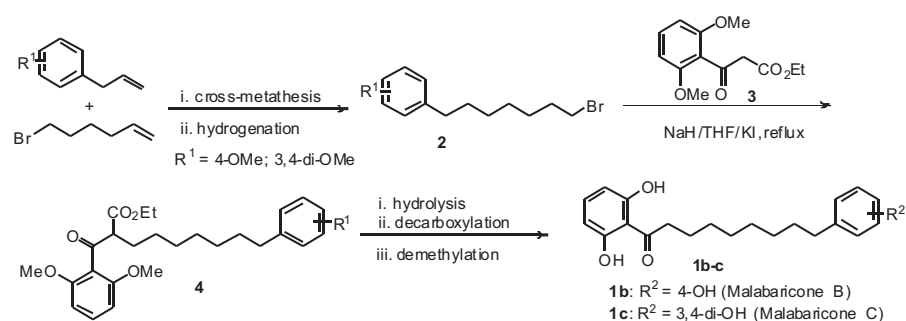
Earlier, malabaricones, isolated from fruit rind of *Myristica malabarica* has been used for performing pharmacological studies in our laboratory. However, isolation of these compounds from plant extract has always remained tedious since the whole malabaricone family is chemically very closely related to each other. Besides, in vitro and in vivo evaluation of malabaricones for studying mechanism of action, pharmacological relevance and therapeutic efficacy warrants a requirement of significant amount of compound. To address this issue, we sought to develop a protocol for syntheses of malabaricones in gram scale.

and transcription of the anti-apoptotic proteins (Fig. 6). Furthermore, analyses of the mitochondrial fractions, of p53 expressing and silenced cells, revealed that cytoplasmic accumulation of glutathionylated p53 (p53-SSG) and p65 (p65-SSG) trigger a robust mitochondrial death process.

Therapeutic efficacy of mal C alone and in combination with NAC in vivo tumor models

Considering impressive anti-cancer potential of mal C alone and in combination with NAC in vitro, their efficacy was evaluated using a lung tumor xenograft mouse model. Tumor bearing mice were administered orally with vehicle e, mal C (100 mg/kg body weight), NAC or combination. As shown in Fig. 7 A-D, oral administration of mal C alone (100 mg/kg) resulted in significant reduction in both tumor volume and weight but the

combination of mal C and NAC resulted in the most effective response in terms of tumor growth retardation compared to vehicle treated mice. In order to evaluate the anti-tumor efficacy against aggressive and nonresponsive tumors, we used B16F10 C57BL/6 murine melanoma tumor model. B16F10 melanoma tumors are aggressive, highly invasive and metastasizes to lungs. Interestingly, mal C dose (50 and 100 mg/kg body weight) dependently reduced both tumor volume and weight. Moreover, combination of mal C and NAC resulted further



Scheme 1. Total synthesis of malabaricone B and C via cross-metathesis strategy

Olefin cross-metathesis has emerged as the most powerful catalytic carbon-carbon bond forming reactions leading to profound synthetic developments in the materials, agricultural, and pharmaceutical industries. This strategy has been successfully utilized in synthesis of ω -arylheptyl bromide (2), one of the key building blocks of our synthetic strategy (Scheme1). Successful C-alkylation of 3, with 2 was achieved in presence of base and KI as an additive to obtain the β -ketoester (4). Compound 4 was then converted to mal B (1b) and mal C (1c) by means of alkaline hydrolysis, decarboxylation followed by demethylation (Scheme 1). The present protocol can be adopted for the synthesis of all other members of malabaricone family, including mal A (1a) and mal D (1d). Concise synthetic route using readily available inexpensive starting materials, high overall yield and simpler reaction conditions are some of the prominent features of our synthetic strategy. The cytotoxic properties of the synthesized mal B and mal C were found to be similar to those isolated from the natural resources.

Library synthesis of malabaricones analogues for structure-activity relationship study towards the development of most potent cytotoxic agent

Our studies revealed that mal C demonstrates anti-tumor properties with the potential for cancer treatment either alone or in combination with other agents, as observed in the breast, lung, colorectal, osteosarcoma and melanoma cancer. Besides, mal C shows higher therapeutic efficacy than curcumin and resveratrol against multiple cancer cells. In order to further ameliorate the therapeutic potential of mal C, we sought to

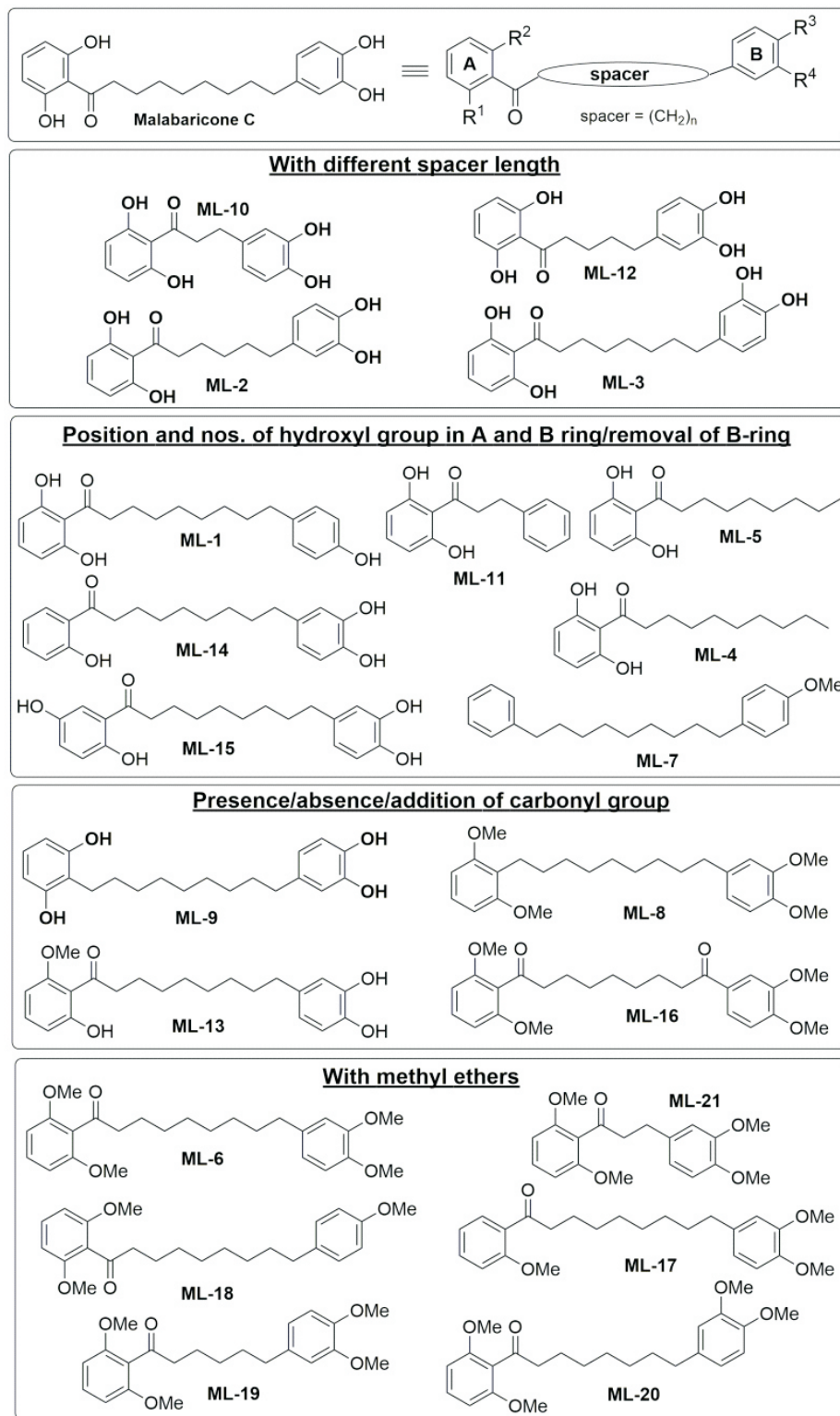


Fig. 8. Library of malabaricone analogues (ML-1 to ML-21) synthesized

understand the role of its different structural attributes in governing the cancer cell death process. We envisaged that the activity of mal C (Fig. 8) can be augmented by modifying its structure in the following ways such as (i) altering spacer length (ii) altering position and number of hydroxyl groups in its A and B ring (iii) removal of the B-

ring and (iv) addition/removal of the carbonyl functionality. To this end, a series of malabaricone analogs (Fig. 8, ML-1 to ML-21) were synthesized by reacting different phenyl β -ketoesters and ω -aryl alkyl bromides/alkyl bromides by following our protocol used in synthesis of mal B and mal C.

Evaluation of in vitro anti-cancer potentials of these analogues revealed

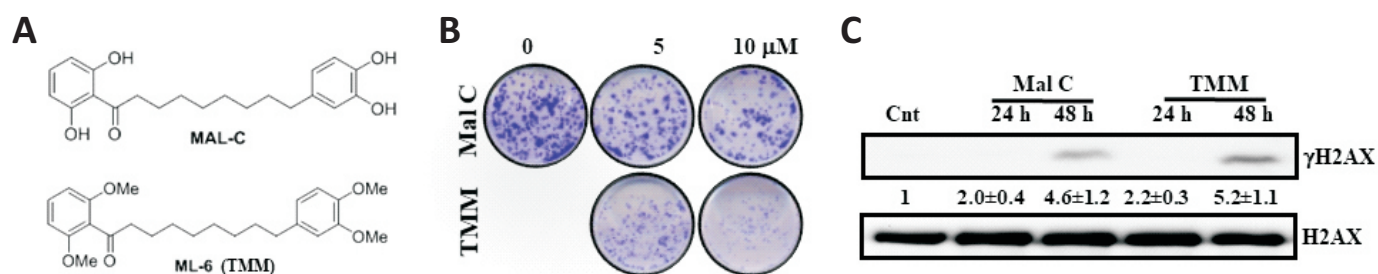


Fig. 9. Breast cancer cells were treated with (A) mal C and TMM and their ability to (B) inhibit clonogenic growth and (C) induce double strand breaks was assessed. γ H2AX is the marker for double strand breaks.

that altering the functional groups in ring-A, -B, carbonyl group or change in aliphatic carbon chain length significantly reduced breast cancer killing potential of mal C. However, amongst the analogues, the new tetramethoxy malabaricone (TMM, ML-6, **Fig. 9**) was more effective in inhibiting tumor cells growth when compared to mal C. In clonogenic assay, the TMM showed IC₅₀, which is 3 fold smaller than mal C. Besides, TUNEL assay, Annexin-V staining, caspase activation and PARP cleavage analyses unveiled the ability of TMM to cause breast cancer death by triggering apoptosis. Further our detailed mechanistic evaluation revealed that TMM mediated higher cell death is associated with induction of DNA double strand breaks, abrogation of G2/M checkpoint and blockage of cell survival process i.e., autophagy (**Fig. 9**).

Conclusions

Natural products have always been an important source of bio-active compounds, and for the last several years, Bio-Organic Division, BARC, is deeply engaged in the development of phytochemicals as anti-cancer agents. To this end, an important polyphenolics viz. malabaricone C (Mal C), which was isolated from fruit rind of rampatri spice displayed impressive anti-cancer properties in vitro and in vivo tumor models. Mal C alone and in combination with NAC effectively reduced lung and melanoma tumor burden in preclinical mice

models. Mechanistically, thiol antioxidants targets "catechol-quinone redox cycle" of mal C to generate copious amounts of ROS and cause higher DNA DSBs. Besides, thiol antioxidants cause glutathionylation of survival proteins, accumulation in cytoplasm and mitochondrial death process in response to mal C treatment.

Keeping in view the involvement of laborious procedure for the extraction of malabaricones from plant matter as well as the requirement of larger amount of them for elucidation of their mechanism of action, an innovative protocol of their synthesis was earlier developed by us [18].

Furthermore, a library of malabaricone analogs was synthesized to evaluate the correlation of various functional groups with their biological activities which in turn will be useful in designing malabaricone congeners with improved cytotoxic efficacy. Gratifyingly, it was observed that tetramethylether of mal C (TMM) (devoid of any phenolic OH group), the synthetic precursor of mal C, and displayed better cytotoxicity against breast cancer than that obtained with mal C.

This has prompted us to carry out detail investigation on the mechanism of their action, which is currently underway.

Corresponding authors and email:
Dr. Sandip K. Nayak (sknayak@barc.gov.in) and Dr. Birija Sankar Patro (bisank@barc.gov.in)

References

1. International agency for research on cancer, WHO, Globocan data (<http://gco.iarc.fr>)
2. F.Tas, Metastatic behavior in melanoma : timing, pattern, survival, and influencing factors, J. Oncol. 647684, 2012, 1-9.
3. S.-J. Soong, R.A. Harrison, W.H. McCarthy, M.M. Urist, C.M. Balch, Factors affecting survival following local, regional, or distant recurrence from localized melanoma, J Surg. Oncol. 67(4) 1998, 228-233.
4. G. Housman, S. Byler, S. Heerboth, K. Lapinska, M. Longacre, N. Snyder, S. Sarkar, Drug resistance in cancer: An overview, Cancers 6, 2014, 1769-1792.
5. M.S. Donaldson, Nutrition and cancer: A review of the evidence for an anti-cancer diet, Nutr. J. 3, 2004, 1-21.
6. A. Bhanot, R. Sharma, M.N. Noolvi, Natural sources as potential anti-cancer agents: A review, International Journal of Phytomedicine 3, 2011, 9-26.
7. W.C. Willett, Balancing life-style and genomics research for disease prevention, Science 296, 2002, 695-698.
8. B.S. Patro, A.K. Bauri, S. Mishra, S. Chattopadhyay, Antioxidant activity of Myristica malabarica extracts and their constituents,

- J. Agr. Food Chem., 2005, 53, 6912-6918.
9. D. Banerjee, A.K. Bauri, R.K. Guha, S.K. Bandyopadhyay, S. Chattopadhyay, Healing properties of malabaricone B and malabaricone C against indomethacin-induced gastric ulceration and mechanism of action, Eur. J. Pharmacol. 578, 2008, 300-312.
10. B. Maity, S.K. Yadav, B.S. Patro, M. Tyagi, S.K. Bandyopadhyay, S. Chattopadhyay, Molecular mechanism of the anti-inflammatory activity of a natural diarylnonanoid, malabaricone C, Free Radic. Biol. Med. 52, 2012, 1680-1691.
11. D. Banerjee, B. Maity, A.H. Bandyopadhyay, S.K. Bandyopadhyay, S. Chattopadhyay, Angiogenic and cell proliferating action of the natural diarylnonanoids, malabaricone B and malabaricone C during healing of indomethacin-induced gastric ulceration, Pharm. Res. 25, 2008, 1601-1609.
12. J.S. Rathee, B.S. Patro, L. Brown, S. Chattopadhyay, Mechanism of the anti-hypertensive property of the naturally occurring phenolic, malabaricone C in DOCA-salt rats, Free Radic. Res. 50, 2016, 111-121.
13. B. Norden, P. Lincoln, B. Akerman, E. Tuite. In metal ions in biological systems: Probing of Nucleic Acids by Metal Ion Complexes of Small Molecules; Sigel, A., Sigel, H., Eds.; MerceL Dekker: New York, 1996, Vol. 33, 177-252.
14. D.S. Sigman, A. Majumder, D.M. Perrin. Chemical nucleases, Chem. Rev. 93, 1993, 2295-2316.
15. B.S. Patro, M. Tyagi, J. Saha, S. Chattopadhyay, Comparative nuclease and anti-cancer properties of the naturally occurring malabaricones, Bioorg. Med. Chem. 18, 2010, 7043-7051.
16. M. Tyagi, B.S. Patro, S. Chattopadhyay, Mechanism of the malabaricone C-induced toxicity to the MCF-7 cell line, Free Radic. Res. 48, 2014, 466-477.
17. M. Tyagi, R. Bhattacharyya, A.K. Bauri, B.S. Patro, S. Chattopadhyay, DNA damage dependent activation of checkpoint kinase-1 and mitogen-activated protein kinase-p38 are required in malabaricone C-induced mitochondrial cell death, Biochim Biophys Acta Gen Subj. 1840, 2014, 1014-1027.
18. K. Kundu and S. K. Nayak. Total syntheses of malabaricones B and C via a cross-metathesis strategy. J. Nat. Prod. 80, 2017, 1776- 1782.

Biodosimetry Techniques and the Biological Indicators of Radiation Exposure in Humans

Nagesh N. Bhat, Rajesh Chaurasia, Usha Yadav, B. K. Sapra

Radiological Physics and Advisory Division
Health, Safety and Environment Group,
Bhabha Atomic Research Centre, Mumbai-400085

Abstract

Biodosimetry analysis helps in ascertaining the exposure and quantifies the radiation dose using biological indicators of radiation. It plays a crucial role in medical management of exposed individuals, helps to address triage needs in case of small as well as large scale radiological incidents and is also indispensable part of regulatory investigation of excess exposure. Biodosimetry is the only method available for estimation of dose, when either physical dosimeters become unreliable or not available as in most radiological incidents. Many complex exposure scenarios offer challenges for the dose assessment. No single assay can address all the challenges. Biodosimetry lab of HS&EG, BARC, has established state of art facilities for addressing these challenges and developed many indigenous facilities for achieving required throughput. Many innovative methods are developed to address the various logistics of processing, preparation of slides, scoring and reporting of dose estimates.

Keywords: Biodosimetry, Excess exposure investigation, Radiation monitoring, Emergency preparedness, Cytogenetic assays.

Introduction

Biological indicators of radiation exposure heavily rely on scientific investigations for assessment of dose to exposed individuals in the instances of i) regulatory requirement in case of suspected over-exposures indicated by personal monitoring devices, ii) reportable radiological incidents as in malfunction of radiation devices and iii) triage management in radiological emergencies involving large number of individuals. In most of the radiation incidents, physical dosimetric information is rarely available. Besides, most of the accidental exposures are non-uniform involving either partial body or localized exposure to significant doses. In such situations, physical dosimetry may give unreliable dose estimates. Depending on the scenario, biological, internal and clinical dosimetry techniques are applied for reliable dose estimation (Fig. 1).

However, no single biological indicator can fulfill all the

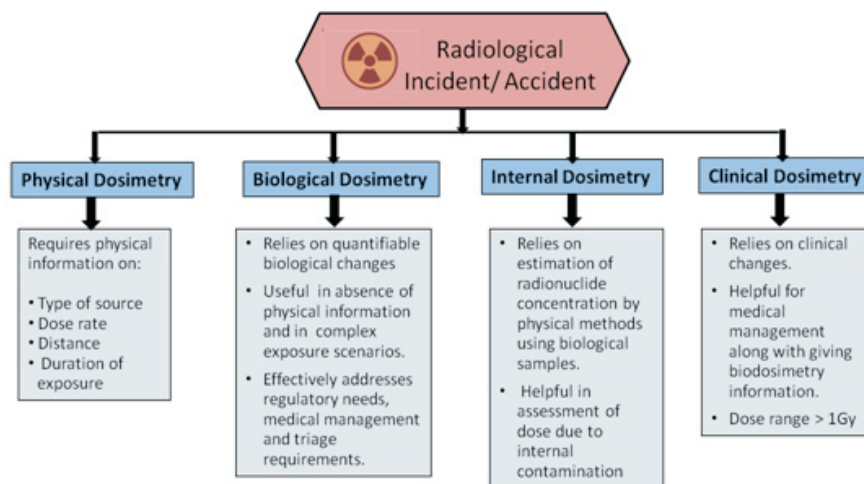


Fig. 1: Various methods employed to investigate excess exposure situations

Table 1: Ideal characteristics of a biological dosimetry technique

1. Sensitivity in a wide dose range of 20 mGy to several Gy
2. Based on observing and analyzing a radiation specific change
3. Changes must occur early but remain stable for long durations
4. Response to all types of radiation (Low/high LET)
5. Reproducible dose response
6. As far as possible, the technique should be non-invasive
7. It should have good repeatability
8. Rapid, simple and amenable to automation
9. Partial body irradiations must be detectable and should enable the part and proportion of body exposed to be identified accurately along with the estimate of dose to the exposed part

requirements to meet challenges of dose estimation, owing to complexities of exposure scenarios. Nonetheless, depending on the need, a particular assay or combination of

assays can help to address the requirements. Often, it becomes necessary to adapt multi-parametric approach to estimate the exposure. This helps eliminate limitations

associated with some assays and also to ascertain exposure levels independently by a set of assays.

In general, the dosimetric information is derived by a combination of several different methods. Although some of the indicators may be purely qualitative or semi-quantitative, they have potential to serve as prognostic indicators. A summary of the different biological indicators and their specific usefulness under different exposure conditions is presented in **Table 2**. Many of these techniques are sensitive to radiation exposure but due to their non-specificity to radiation exposure alone, their application is limited to either as supplementary techniques or in special scenarios.

Few of the cytogenetic changes have been proven to exhibit very good radiation specificity thereby qualifying them as very good indicators for biodosimetry. In particular, dicentric chromosomal aberration assay (DCA), based on identification of dicentrics, is proven to be highly specific to radiation exposure with minimum detectable limit of about 100 mSv. DCA involves many biological processing steps, most of which need aseptic conditions demanding stringent requirements of class II type biological laboratory. The Biodosimetry Lab at BARC has established this technique and developed the SOP for radiation dose assessment. Over the years, cases in excess of 1300, have been referred to this lab for analysis, including radiation workers and members of public in suspected and accidental exposures. Biodosimetry analysis was carried out to estimate doses to exposed individuals during many small scale radiation accidents, one such being the radiological incident

Table 2: Various biological indicators of radiation exposure

1. Prodromal syndrome (radiation sickness)
2. Haematological changes lymphocytes / granulocytes (Day of 500)
3. Cytogenetic changes:
 - Dicentric chromosomes
 - Ring chromosomes
 - Acentric chromosomal Fragments
 - Translocations (reciprocal and non-reciprocal)
 - Insertions and Deletions
 - Micronuclei
 - Neoplastic Bridge
 - γ H2AX and 53BP1 foci
 - The Pseudo-pelger Huët Neutrophil
4. Biochemical Indicators
 - Urinary excretion of 17-ketosteroids
 - Creatine/creatinine ratio
 - β amino isobutyric acid
 - Other amino acids
5. EPR and OSL studies with tooth enamel, bone, hair, and nails
6. Somatic Mutation Assay
 - Glycophorin assay (RBC)
 - HGPRT mutation assay (lymphocytes)
 - Globin assay (RBC)
7. Sperm analysis -reduction in sperm counts 40 days after the exposure
8. Damage to hair follicles
9. Neutron Activation Analysis - ^{24}Na , ^{32}P in biological samples
10. Thermography and scintigraphy (contact thermography, Infrared thermogrammetry to detect exposure of extremities, Radiation scintigraphy to assess the severity of the injury and in follow-up during recovery)
11. Neurophysiological Dosimetry (By EEG variations)

at Mayapuri, New Delhi, in 2010.

Additionally, several research studies are being carried out to address the complex nature of radiation accidents such as non-uniform exposures, protracted exposures with varying dose rates, chronic exposure, life-style confounding factors and retrospective or follow up assessments. These cytogenetic techniques used for biodosimetric evaluations are briefly described below

Dicentric Chromosomal Aberration (DCA) analysis

Chromosomal aberration analysis based on the frequency of dicentric chromosomes (DCA) in cultured peripheral blood lymphocytes is so far the most reliable and universally adopted biological dosimetric technique and termed as the “gold standard” (1). Doses over a wide range of 0.1 -6 Gy can be detected by

this technique. Following acute radiation exposure, dicentric frequency remains unaltered for several weeks, but decays to half the value in around 180 days. Subsequent reduction in the signal occurs slowly with an approximate half-life of 3 years, as seen in the case of low dose and chronic exposures. Hence, doses from past exposures can be assessed with reasonable reliability by applying appropriate correction factors.

The protocol for DCA is described in **Fig. 2**. The microscopic observation of human chromosomal spread post slide preparation can be seen in **Fig. 3**.

The background dicentric frequency in unexposed blood samples is in the range of 0.0005 to 0.001. The frequency increases with dose linear-quadratically for low LET radiations and linearly for neutrons and high

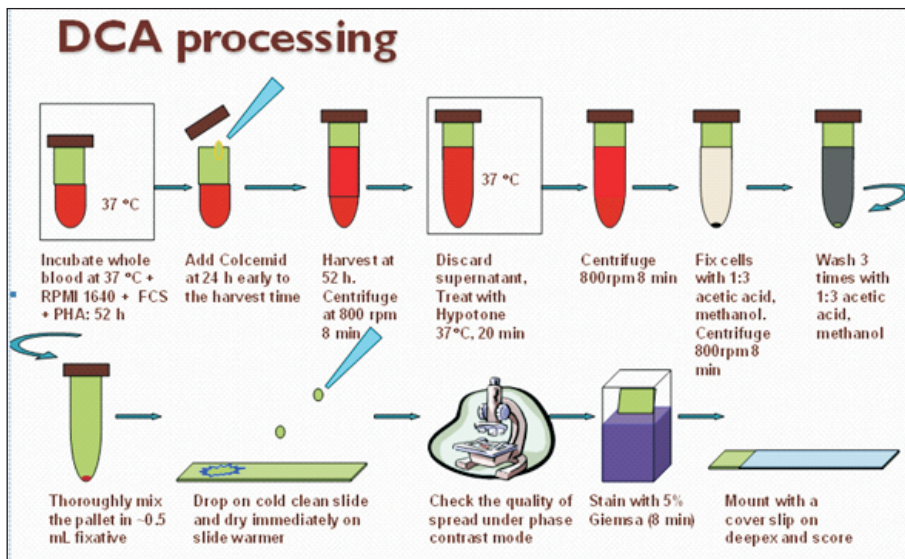


Fig. 2: Protocol for biological dosimetry by chromosome aberration Analysis

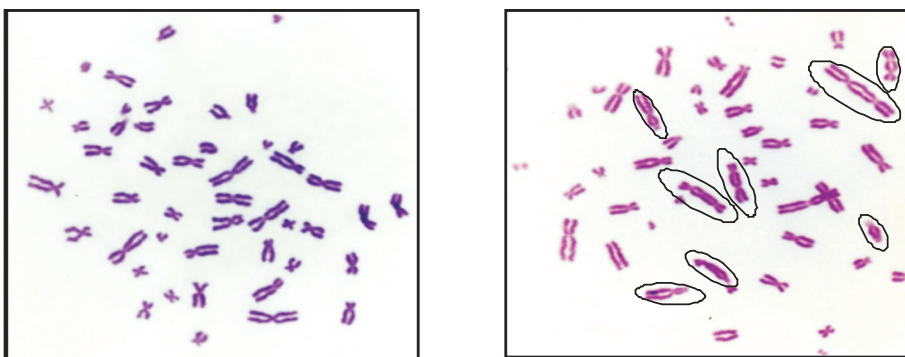


Fig. 3: Representative images of metaphase spread of human chromosomes; spread of a normal unexposed cell (Left) and cell exposed to ionizing radiation containing multiple dicentrics (Right).

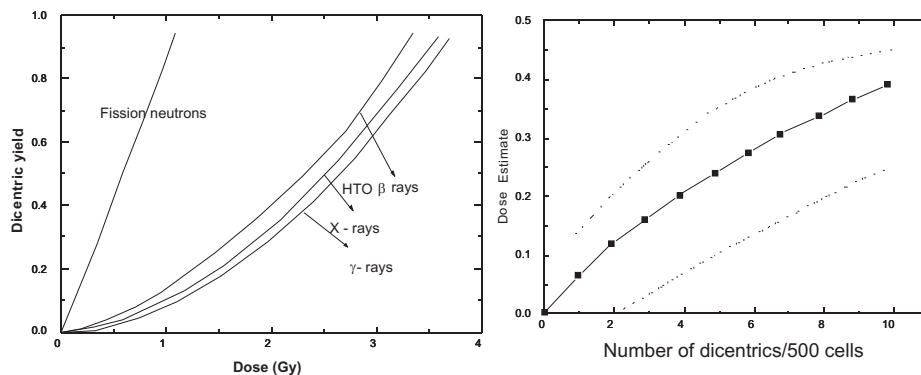


Fig. 4: Calibration curves for DCA (Left) - The curves showing variation in the effectiveness of high and low LET radiation (neutrons and all others respectively). Calibration curve for γ -radiation plotted with upper and lower confidence intervals (Right) - At low doses, low frequency of dicentrics results in relatively high Poisson error leading to large confidence intervals.

LET radiations. The frequency of dicentrics "y" varies with the dose "D" as follows:

$$y = c = \alpha D + \beta D^2$$

The linear (α) and quadratic (β) coefficients are characteristic of the type of radiation. Generally, 500 metaphases are scored per sample

and the frequency of dicentrics y is determined. Absorbed dose is assessed from the relationship,

$$D = \frac{-\alpha + \sqrt{\alpha^2 + 4\beta y}}{2\beta}$$

This dose refers to the equivalent whole body dose received acutely in an accidental exposure. The lower

limit for detection is 50 mGy for X-rays, 100 mGy for γ -radiation and 10 mGy for fast fission neutrons. The calibration curves for different radiations are shown in Fig. 4.

One of the most crucial requirements of this technique is the scoring of the dicentrics by a well-experienced scorer. Further, the scoring of dicentrics is not only time consuming, but also not amenable to automation by signal processing systems due the complexities in the image of dicentrics w.r.t their physical characteristics. Recent advances such as metaphase scanners and centromere painting by antikinetocore antibodies or nucleic acid probes can enhance the scoring speed and reduce errors in the identification of dicentrics. In accidents involving exposures in the lethal range (3-6 Gy), it suffices to score 25-50 metaphases for providing the preliminary information required for medical management of victims. However, at higher doses most of the severely damaged cells fail to go through the cell division and it may be very difficult to find even a few metaphases. Hence, when low doses of the order of a few 100s of mGy have to be detected, the Poisson error associated with the estimates can be very large since only a few dicentrics are available for estimation.

In uniform whole body exposures, the radiation induced dicentric chromosomes follow a perfect Poisson distribution. However, in most accidents the exposures is non-uniform, resulting in a fraction of lymphocytes receiving a much larger dose as compared to those in the unexposed part of body. As a result, the total aberrations scored are concentrated in a few damaged cells, which reach the metaphase. The degree of over-dispersion can be assessed by the dispersion

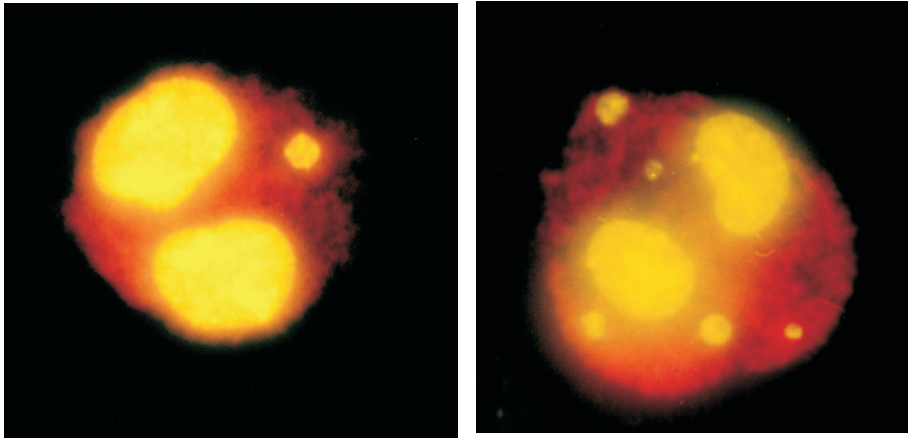


Fig. 5: Representative images of cytokinesis blocked bi-nucleated cells containing one and five Micronucleus Assay (MN assay).

coefficient u .

$$u = \frac{[\sigma^2/y - 1] [N - 1]}{\sqrt{2(N - 1)(1 - 1/Ny)}}$$

Where, N is the total number of cells scored; y the frequency of dicentrics and σ^2 its variance. A positive, negative or a zero value of u indicates over-dispersion, under-dispersion and a perfect Poisson distribution respectively. In accident situations, a value greater than 1.96 suggests a partial body or localized exposure.

Micronucleus Assay (MN assay)

Micronuclei refer to small nuclei formed from the chromatin material which lags behind and does not get included in either of the daughter nuclei formed during cell division (Fig. 5). Exposure to radiation and other clastogenic agents results in a

dose dependent increase in the frequency of MN (2, 3). Dividing cells are blocked at cytokinesis using cytochalasin B, in order to visualize the induced MN.

Even though there are claims that MN assay can detect absorbed doses of the order of 50 mGy, large individual variations in background frequency do not permit reliable estimates of doses less than 0.25 Gy. In accident situations involving absorbed doses in the range of 2-6 Gy, very reliable information can be obtained within 3 days after the exposure. In accidents involving exposure to a large number of people, MN assay may be particularly useful, when well-trained technicians are not available to score dicentrics. The prospects of automation are much better for MN assay as compared to DCA.

Premature Chromosome Condensation (PCC)

Conventionally, to study chromosomal aberrations, like in dicentric assay, lymphocytes are first stimulated to divide and then arrested at metaphase stage. The process takes a minimum of 48h after blood withdrawal. Moreover, at high dose exposures, obtaining cells at metaphase becomes difficult due to cell cycle arrest at G2/M checkpoint and severe leucopenia. In such cases to visualize aberrations, chromosome condensation is induced artificially at interphase stage itself by methods called premature chromosome condensation or PCC.

There are two means of inducing PCC: 1. Drug induced PCC in which chemicals such as Calyculin-A, and Okadaic Acid, are used to induce condensation efficiently in cells arrested at G2 phase by allowing them to enter prematurely in mitosis. 2. Fusion induced PCC in which chromosomes are condensed artificially in resting G0 phase itself, without culturing them for 48h.

In this process, chemical factors responsible for chromosome condensation are transferred in the cells by fusing them to mitotic cells.

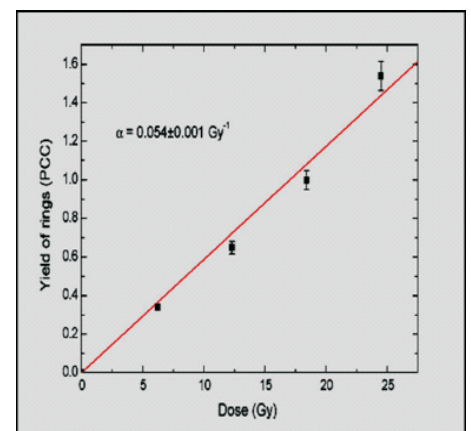
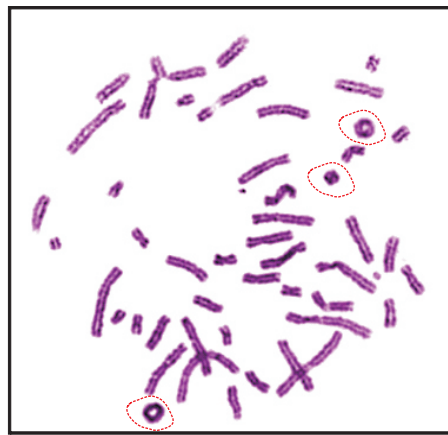
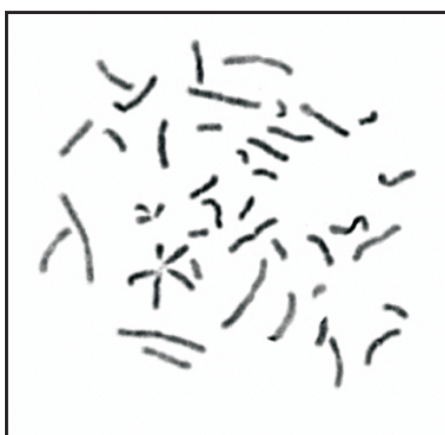


Fig. 6: Chromosomal spreads analyzed in PCC-Ring assay - Unexposed spread shows all linear chromosomes (left) and the spread containing three hollow ring chromosomes induced by radiation is seen in the centre image. The linear dose response curve for frequency of ring chromosomes induced by Co-60 gamma radiation (Mutation Research 699 (2010) 11-16) is shown in the image on the right.

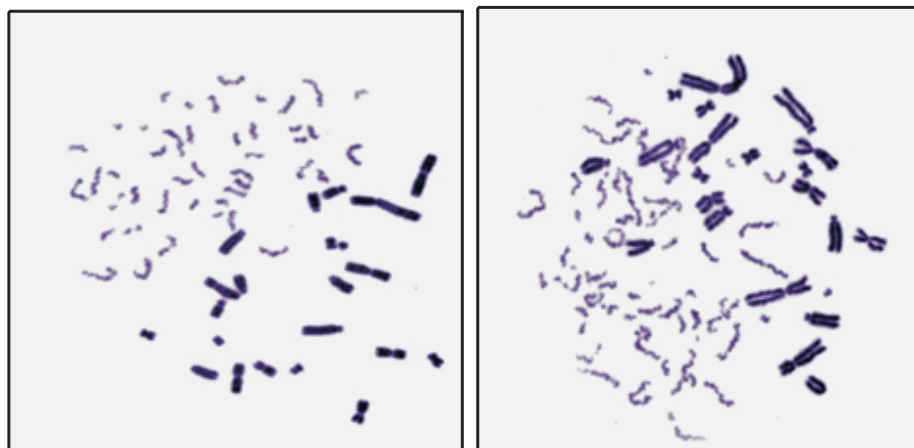


Fig. 7: Representative images of spreads showing cell fusion induced premature chromosome condensation. Unexposed samples show most of the spread with normal count of 46 chromosomes (left), whereas, exposed spreads contain bodies excess to 46 (right).

Fluorescence in situ hybridization (FISH) assay

Radiation induced unstable chromosomal exchanges like the dicentrics, rings and deletions, decay with a $T_{1/2}$ of 1-3 years depending upon the exposure condition. As a result, there is a considerable uncertainty in this dosimetry for past exposures. Scoring stable chromosomal exchanges such as reciprocal chromosomal translocations is a possible approach to overcome this problem (6). Conventionally, chromosomal banding technique, which is very tedious and time-consuming, is used for scoring translocations. Recently, the availability of whole chromosome specific libraries has enabled painting of individual chromosomes by FISH technique. This assay not only makes the identification of translocations very easy, but also increases the sensitivity by its ability to score events, which the conventional banding may fail to detect. The various types of FISH applications pertaining to biodosimetry are listed below.

Whole chromosome painting and centromere FISH

Translocations involving exchange of parts between the painted

Drug induced PCC-Ring assay

Blood collected from the subject is cultured as in case of DCA for 48-52h and PCC inducing chemical Calyculin-A (50nM) is added for the last one hour of the culture. Processing and slide preparation is similar to DCA. Chromosomal spreads from every phase of mitosis can be seen. Hollow ring chromosomes induced by radiation are beautifully visible in this assay and the frequency of the same is used for dose estimation (Fig. 6). Radiation dose response curve has been prepared by in-vitro experimentation and it has been found to be linear in the range of 5-15Gy (4).

Cell fusion based PCC

The method has been established recently in our lab and multiple aspects of the same are being explored. In this method, blood cells from the subject are fused to mitotic cells. The mitotic cells are Chinese hamster ovary cells already cultured and arrested in metaphase which retain chromosome condensation factors. The process of fusion and condensation takes around 3h and then the sample is processed for slide preparation. Dose estimation can be quickly carried out using excess chromosomal fragment analysis (Fig. 7). In addition, this technique can be combined with fluorescent in situ hybridization for quantification based on many more endpoints such as Dicentrics, translocation (5).

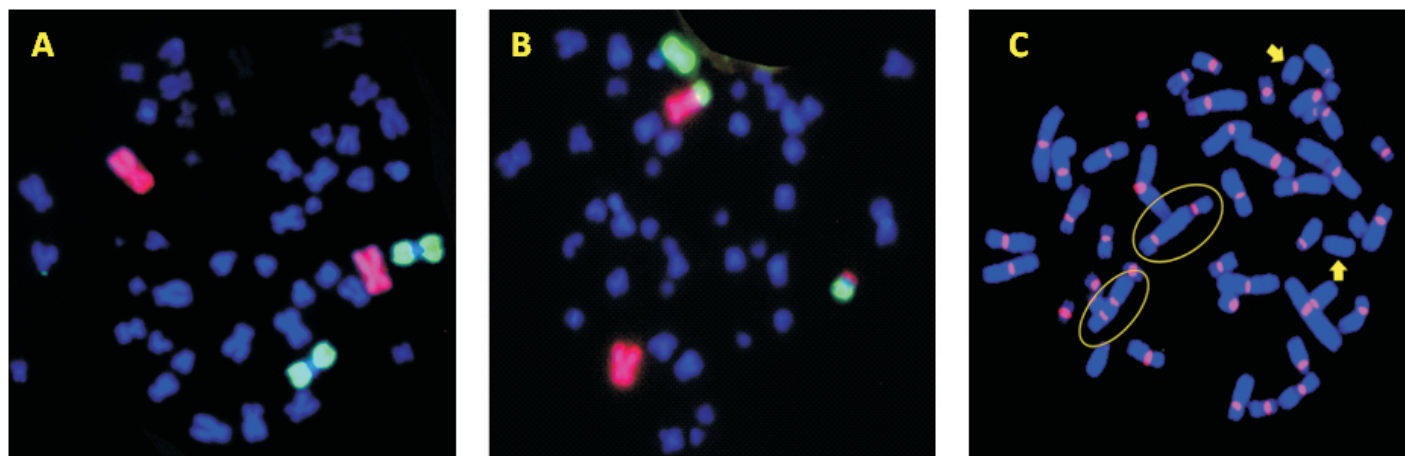


Fig. 8: Representative pictures of bicolour FISH: (A) Normal metaphase spread showing Chromosome pair 1 and 2 painted with green and red probes respectively (B) metaphase spread with reciprocal translocation between chromosome 1 and 2. (C) Centromere painting with PNA (Peptide Nucleic Acid) probe for the detection of dicentric chromosomes (illustrated in yellow circle).

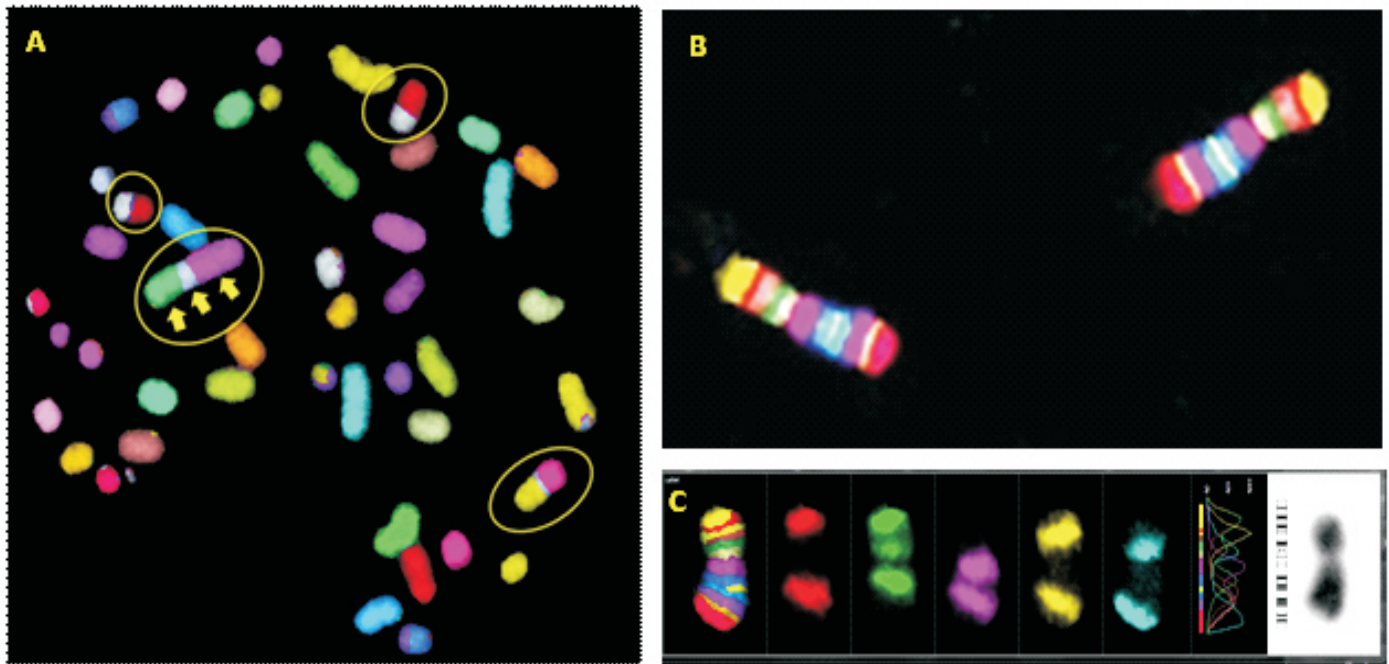


Fig. 9: (A) mFISH metaphase spread exposed to 4Gy of ⁶⁰Co- γ-rays, inter-chromosomal translocations are marked in circle. (B & C) mBAND FISH of normal chromosome no. 2: images captured using different optical filters and a final superimposed image.

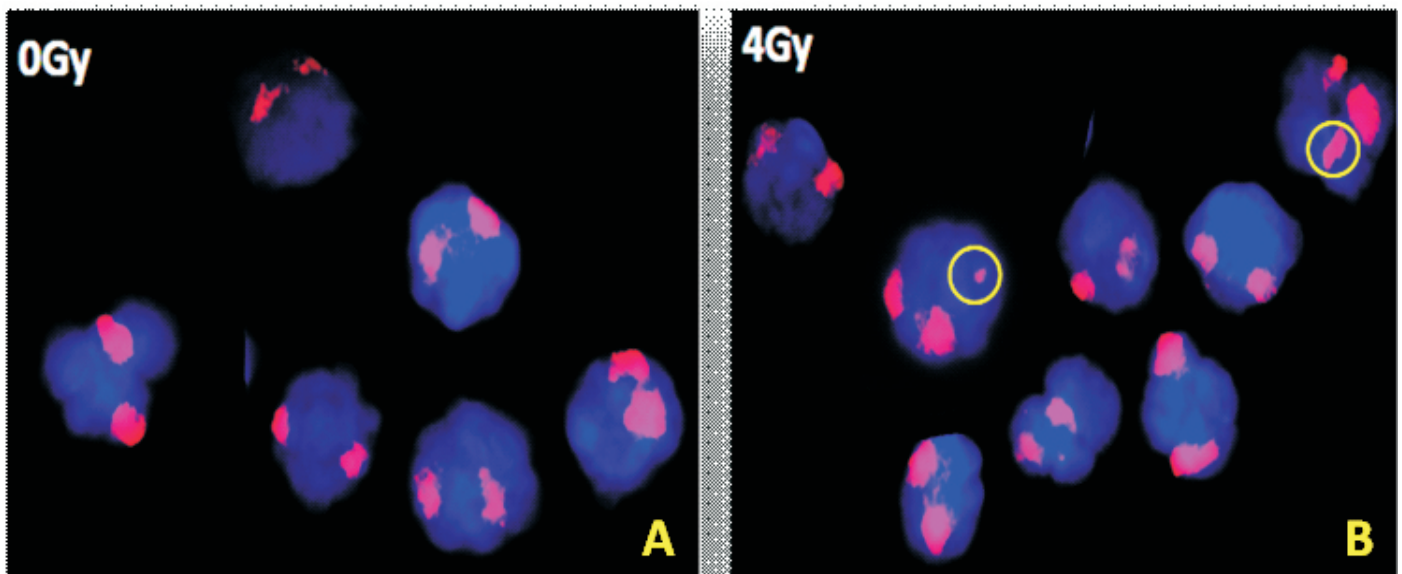


Fig. 10: G0-FISH; (A) normal human lymphocytes, first pair of whole chromosome painted with red probes, no translocation observed, (B) human lymphocytes exposed to 2 Gy of ⁶⁰Co-γ-radiation, 2 translocations can be seen in this microscopic field view illustrated in yellow circle.

chromosomes and counter-stained (unpainted) chromosomes are visualized as bicoloured structures (Fig. 8 A & B). Since only a part of the genome is painted (10-20%), the information for the whole genome is derived by extrapolation of the response obtained for the painted fraction. Since it is likely that individual chromosomes may differ in their radiosensitivity, there is a need to obtain calibration curves with

different cocktails of painted chromosomes.

The FISH technique can also be used to visualize and confirm the dicentrics by staining of centromeres with fluorescence probes. This is advantageous over the conventional tedious method which uses classical Giemsa staining. Development of peptide nucleic acid (PNA) probes makes this job precise and easy. PNA probes exclusively bind with the

centromere region of all the chromosomes making the detection and quantification of dicentrics more efficient. A typical spread showing dicentrics stained with PNA centromere probes is shown in Fig. 8C.

Multicolour (m-FISH) and multicolour banding (m-BAND) fluorescence in situ hybridization

m-FISH and m-BAND are advanced chromosome painting tools, dealing

with multiple chromosome or region-specific paint-probes in one step. m-FISH offers painting of all 23 pairs of chromosomes with different colours and helps in the detection of inter chromosomal exchanges. The different regions of the chromosome get painted with different colours in the mBAND FISH technique which facilitates the detection of rearrangement within the body of the same chromosome. While the intra-chromosomal rearrangements are predominantly induced by High LET radiation, Low LET radiations generally lead to inter-chromosomal rearrangements. The images showing the painted chromosomes as seen by the mFISH and mBAND techniques are shown in Fig. 9.

Interphase (G0) FISH

This technique does not require cell culturing as it deals with detection of translocations/fragmentation at interphase stage itself. High doses of radiations are capable enough to induce heavy damage to the cellular metabolic machinery; as a result, the cell may not be able to enter in the process of cell division even with the treatment of high concentrations of mitogens. Any pair, arm or region of the chromosome can be painted for visualization of the radiation induced chromosomal translocations/fragmentation. Fig.10A shows the images of G0 phase lymphocytes showing red spots corresponding to pair of chromosome 1, Fig. 10B with extra spots indicating fragment or translocation of the chromosome.

Proteomic Biodosimetry Markers

γ H2AX Assay

This assay has been projected as a promising assay in the recent days for quick biodosimetry. It employs the detection of γ H2AX foci which are formed due to double strand breaks (DSB) of DNA. The detection of the

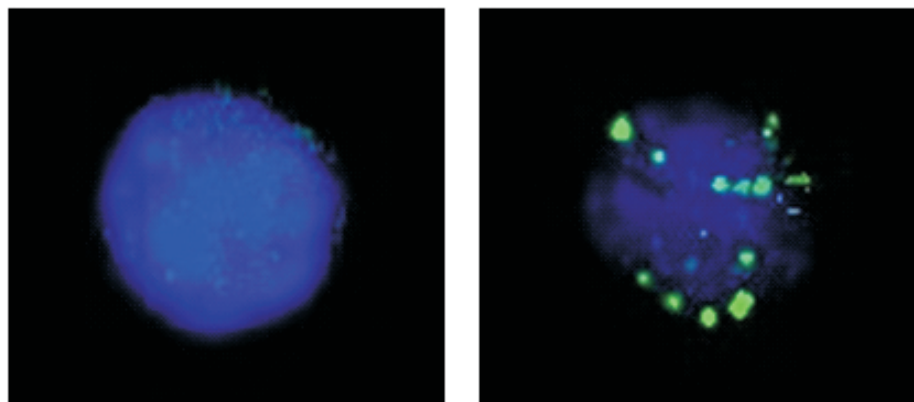


Fig. 11: Representative images of a normal and ionizing radiation exposed cell processed for visualization of γ H2AX foci; (left) Normal cell without γ H2AX foci and Cells expressing γ H2AX foci (right).

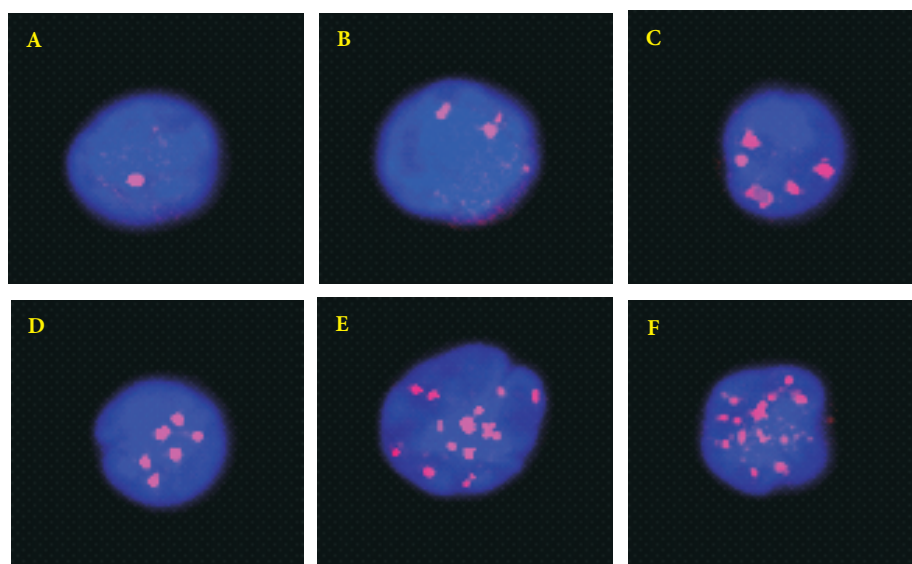


Fig. 12: Representative images of cells exposed to low to high doses of ionizing radiation, processed for visualization of 53 BP1 foci (A-F: 0-2 Gy)

foci is by immuno-fluorescent staining methods. In spite of several limitations such as fast decay of biodosimetry signal, uncertainties associated with blood collection delay, and decay of signal during transportation of blood samples, the assay can be used for quick results in case of triage management for classification of exposed individuals for medical management. Few studies have also reported the use of this assay for clinical applications and dose estimation in case of diagnostic exposures involving few 10 mSv of exposure wherein quick blood collection is possible immediately after the exposure. Efforts are being made to develop protocol to arrest the biological process immediately after collection of blood sample by various

fixing methods for easy transport of samples to the analyzing laboratory.

53 BP1 Immunofluorescence Assay

Like γ -H2AX, phosphorylated-53BP1 is another proteomic marker of DSB, being used as a rapid tool for biodosimetry. Phosphorylated histone H2AX and p53 binding protein-1 (53BP1) are commonly accepted molecular markers of ionizing radiation induced foci. Upon DSB induction, histone H2AX molecules get phosphorylated within chromatin domains containing DSB. 53BP1 is a downstream protein which gets recruited at the site of induced DSBs.

The Pseudo-pelger Huët Neutrophil-A new permanent radiation biomarker

Pseudo Pelger Huet Anomaly (PHA) is a recently discovered in vivo marker of radiation exposure observed in circulating blood neutrophils. Normal neutrophils contain 3 to 4 lobed nucleus whereas PHA is characterized by round, oval, bean-shaped or symmetric bi-lobed nuclei, which are joined by a thin mitotic bridge (7). PHA is commonly known to be induced by a decreased level of expression of the lamin-B receptor (LBR) due to mutation in LBR gene. PHA is specific to in-vivo (formed in the bone marrow) and it cannot be induced ex-vivo (cells getting exposure when they are outside the body). In an analysis of archival peripheral blood slides from the 1958 Y-12 criticality accident (at Oak ridge, Tennessee, USA), authors have shown that the PHA morphology appeared within 12

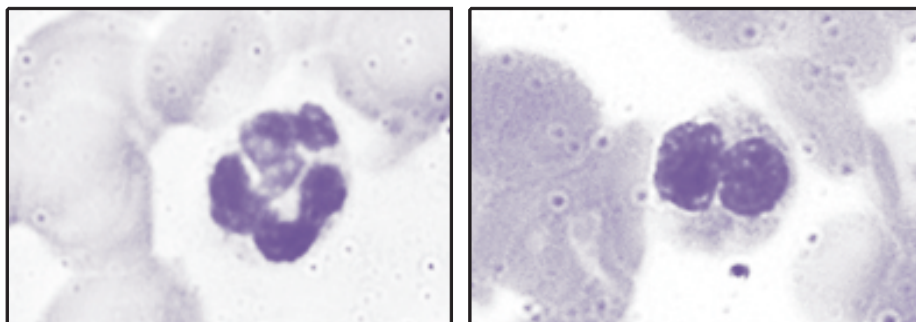


Fig. 13: Representative images of a normal neutrophil (Left) and other containing PHA i.e., bi-lobed nucleus joined by a thin mitotic bridge (Right)

hours in the circulation after radiation exposure, hence it could be a potent marker of acute radiation exposures. In the same accident, in one of the radiation victims, the PHA marker was persistent up to 16 years, reflecting a stable (permanent) radiation induced mutation marker which can be useful as a retrospective dosimeter. An initiative has been made to establish a dose response curve for PHA, by scoring and

analyzing circulating blood neutrophils of two radiation exposed individuals. Establishment of response curve for PHA is a tedious job as it demands radiation exposed human volunteers. To establish PHA as a potent biodosimeter, worldwide in vivo research is ongoing.

Conclusions

Biodosimetry techniques help to assess and ascertain radiation dose of

Biodosimetry Techniques at a glance

Assay	Dose range	Advantages/applications	Limitations
Dicentric Chromosome Aberration analysis	0.1 – 6 Gy	Radiation specific, very low background, sensitive	Labour intensive, requires skilled manpower, results available only after 72 h.
Micronucleus Assay	0.25 – 6 Gy	Easy to score, amenable to automation.	Not possible to detect non-uniform exposure, relatively high background, inter-individual variation of response and background, longer culture duration (72 h).
Fluorescent <i>in situ</i> hybridization (FISH)	0.25 – 6 Gy	Stable signal for many years, very helpful for retrospective biodosimetry, internal exposure and high LET exposure.	Relatively non-specific, high background, very tedious and lengthy procedure, expensive.
Premature chromosome condensation (PCC) assay	PCC-R assay drug induced 3– 25 Gy	Useful for high-dose exposures, simple to perform, radiation specific (ring chromosomes)	Not suitable for low doses, 48h culture is required, Cell cycle dependent
	PCC-Fusion induced (fragments) 1 - 20 Gy	Quicker results, no cell culture required, useful for high-dose exposures where other assays may fail	Tricky to perform, Not radiation specific
γH2AX assay	0.1 ≤ 6 Gy	Very quick results, amenable to automation, possibility of detecting doses <0.1 Gy with blood samples available immediately after exposure, very high sensitivity, good tool as a clinical application.	Too many confounding factors, signal fades very fast, needs to be performed quickly after exposure, not suitable for protracted exposures, can be only used as a supplementary technique with other assays.

individuals involved in radiation exposure and provide important information needed for both regulatory and medical management. Suspected exposure cases, as indicated by personnel monitoring devices, need to be ascertained by biodosimetry technique to avoid the possibility of spurious cases. Most of the radiation accidents are non-uniform in nature, thereby leading to many uncertainties in measured dose by personnel monitoring devices. In addition, biodosimetry techniques help to assess doses when individuals involved in radiation accidents do not have personal monitoring devices. Due to the complexity of exposure scenarios, one single technique does not suffice the needs; nonetheless, established techniques suffice and effectively address the needs. As a part of investigation process, these techniques have helped to identify and quantify radiation dose to exposed individuals while handling many complex scenarios of excess exposure.

Corresponding author and email:

Dr. Nagesh N. Bhat
(nageshnb@barc.gov.in)

References

1. M.M. Pinto, N.F. Santos, A. Amaral
Current status of biodosimetry based on standard cytogenetic methods, *Radiat Environ Biophys.*; 49(4):567-81. doi: 10.1007/s00411-010-0311-3, Nov.2010.
2. K. Shirsath, N.N.Bhat, K. Anjaria, U. Desai, S. Balakrishnan
Cytokinesis blocked micronucleus (CB-MN) assay for biodosimetry of high dose accidental exposure, *International Journal of Radiation Research*, Vol. 12, No.3, 2014.
3. R.K.Nairy, N.N.Bhat, G.Sanjeev and N.Yerol.
Dose-response study using micronucleus cytome assay: a tool for biodosimetry application, *Radiation Protection Dosimetry* Vol. 174, No. 1, pp. 79–87, 2017.
4. S. Balakrishnan, K. Shirsath, N. N. Bhat, K. B. Anjaria, Biodosimetry For High Dose Accidental Exposures By Drug Induced Premature Chromosome Condensation (PCC) Assay, *Mutation Research* 699, pp.11–16, 2010.
5. I. Karachristou, M.Karakosta, A. Pantelias, V.I. Hatzi, K. Pantelis, P. Dimitriou, G. Pantelias, G. I. Terzoudi, Triage biodosimetry using centromeric/telomeric PNA probes and Giemsa staining to score dicentrics or excess fragments, *Mutation Research* 793 107–11, 2015.
6. A.A. Edwards, C. Lindholm, F. Darroudi, G. Stephan, H. Romm, J. Barquinero, et al. Review of translocations detected by FISH for retrospective biological dosimetry applications. *Radiat Prot Dosim*, 113:396–402, 2005.
7. R. E. Goans et al, appearance of pseudo-pelger huetanomaly after accidental exposure to ionizing radiation in vivo, *Health Phys.* 112(3):252–257, 2017.



Central Complex BARC

Edited & Published by:
Scientific Information Resource Division
Bhabha Atomic Research Centre, Trombay, Mumbai 400 085, India
BARC Newsletter is also available at URL:<http://www.barc.gov.in>